TR - H - 086

Using an Inverse Dynamics Representation to Reconstruct Temporal Firing Patterns of Purkinje-cells in Monkey Ventral Paraflocculus

Hiroaki GOMI
(NTT Basic Research Labs.)

Munekata SHIDARA
(Electrotechnical Lab.)

Aya TAKEMURA
(Electrotechnical Lab.)

Yuka INOUE
(Electrotechnical Lab.)

Kenji KAWANO
(Electrotechnical Lab.)

Mitsuo KAWATO

1994. 7. 14

ATR人間情報通信研究所

〒619-02　京都府相楽郡精華町光台2-2　☎ 0774-95-1011

ATR Human Information Processing Research Laboratories
2-2, Hikaridai, Seika-cho, Soraku-gun, Kyoto 619-02 Japan
Telephone: +81-774-95-1011
Facsimile: +81-774-95-1008

Using an Inverse Dynamics Representation to Reconstruct Temporal Firing Patterns of Purkinje-cells in Monkey Ventral Paraflocculus

Hiroaki GOMI*
Munetaka SHIDARA**
Aya TAKEMURA**
Yuka INOUE**
Kenji KAWANO**
Mitsuo KAWATO***

* NTT Basic Research Laboratories.
** Neuroscience Section, Electrotechnical Laboratory.
*** ATR Human Information Processing Research Laboratories.

Correspondence to:

Hiroaki Gomi

Information Science Research Laboratory,
NTT Basic Research Laboratories.
3-1 Morinosato, Wakamiya, Atsugi-Shi, Kanagawa Pref., 243-01 JAPAN
phone: +81-462-40-3581
fax : +81-462-40-4721

Abbreviated title:
Reconstruction of Firing Patterns of P-cells in VPFL

Acknowledgment
We thank Dr. F. A. Miles for his helpful comments and suggestions. We thank Dr. S. Yamane, Dr. Y. Tohkura, and Dr. M. Honda for their continuing encouragement. This works was partly supported by a Grant to K.K. and M.K. from the Human Frontier Science Program.

Abstract

The complex temporal firing frequencies of Purkinje cells (P-cells) in the monkey cerebellum ventral paraflocculus were reconstructed based on a second order linear inverse dynamics representation consisting of eye acceleration, velocity, position, and bias terms. These firing patterns were observed during ocular following responses (OFR) induced by movements of a large-field visual scene. Many P-cell firing patterns (109/232 from 30 P-cells, 16 stimulus conditions) were well reconstructed from eye movements with reliably estimated coefficients by least square error minimization technique with evaluating the modeling error, the fitness of the reconstructed firing frequency and the reliability of the estimated time-lag. Further, two statistical methods show the necessity and sufficiency of the second order model.

From the coefficient analyses, the two types of P-cells (local linearly and global linearly correlated to the eye movements) were found although the nonlinear relations were observed between the stimulus speed and firing frequency in the most of P-cells. The coefficients of a single P-cell independently estimated in several stimulus conditions were close to each other in the P-cells global linearly correlated to the eye movements, and these temporal firing frequencies in several stimulus conditions were successfully reconstructed by one parameter set. This result indicates the generality of this linear inverse dynamics representation for these P-cells. In the local linearly correlated P-cells, the firing frequency tended to be insensitive as the eye velocity increased.

Moreover, the averaged ratio of the acceleration coefficient to the velocity one is close to that in eye motor neurons, suggesting that the dynamic component of the eye driving signal for ocular following response is generated by the P-cells. This result supports the hypothesis that the cerebellum works as a motor command generator which computes an inverse dynamics model for each motor system.

Key words:

ocular following response, cerebellum, Purkinje cell, firing frequency reconstruction, inverse dynamics representation, least square error method.

Contents

1. Introduction

To reveal mechanisms of animal or human coordinated and smooth movements, computational mechanisms in the brain's higher motor center should be investigated not only from physiological aspects but also from the view points of information processing systems. Many lines of experimental evidence have suggested that the cerebellum is involved in motor control. Several research groups have found that different regions of the cerebellum play important roles in the different motor behaviors, such as arm movement, locomotion, posture control, and several kinds of eye movements. See, for example, (Ito, 1984). But what aspects of movements do cerebellar neurons encode quantitatively? And how do they carry the information for movements?

With regard to slow tracking eye movements, the activity of Purkinje cells (P-cells) in the ventral paraflocculus of the cerebellum is known to be correlated with eye velocity (Lisberger & Fuchs, 1978; Miles & Fuller, 1975; Miles, Fuller, Braitman, & Dow, 1980; Stone & Lisberger, 1990) and acceleration (Stone & Lisberger, 1990). These results indicate that the spike firing frequency carries the information of some aspects of the eye movements. However, we need more quantitatively sufficient analysis to discuss the information encoding and effects on eye movements in comparing the characteristics of neural activity in several brain regions.

Neural activities associated with one type of slow eye movements, the ocular following response (OFR) (Miles, Kawano, & Optican, 1986) induced by movements of a large-field visual scene, were reported in several brain regions: medial superior temporal area (MST) (Kawano, Shidara, Watanabe, & Yamane, 1994), dorsolateral pontine nucleus (DLPN) (Kawano, Shidara, & Yamane, 1992), and ventral paraflocculus (VPFL) (Shidara & Kawano, 1993) of the cerebellum. From these studies it was inferred that the neural firings in MST and DLPN encode the visual input signals and that the P-cells send the eye driving signals.

Based on these observations, the reconstruction of Purkinje cell firing frequencies from eye movements during the OFR have been demonstrated in Shidara, Kawano, Gomi and Kawato (1993). The present paper gives extended quantitative analyses of P-cell firing patterns observed in 30 P-cells of three monkeys under 16 conditions: five stimulus speeds in preferred direction, five stimulus speeds in anti-preferred direction, and six stimulus durations (total 232 data sets). To check the suitability of the model and to estimate reliable parameters in the reconstruction P-cell firing temporal frequency, four data classification methods from

different view points were applied. As a consequence, the estimated coefficients were reliable enough to examine the individual local behavior of each P-cell during the OFR. Not only the reliability of estimation, but also the necessity and the sufficiency of the second-order model with position, velocity, and acceleration terms of eye movement was confirmed by statistical parameters, the *p*-values in *t*-test and the Cp-statistics. Moreover, to evaluate the generality of the model for a single P-cell firing, the inverse dynamics representation with one parameter set was used to reconstruct the combined firing patterns observed under several conditions. The nonlinearity of the relation between the P-cell firing and eye movement found in local and global analyses was discussed. This paper also discusses the differences of our method and results from those in previous studies, and discusses a computational hypothesis of the cerebellum as a motor command generator which computes internal models of controlled motor systems.

2. Materials and Methods

2.1 Experimental setup

The experimental conditions are the same as (Shidara & Kawano, 1993) and (Kawano et al., 1992). Briefly, monkeys (*Macaca fuscata*) had been pre-trained to fixate a small target spot in order to obtain a fluid reward. Under Nembutal anesthesia and aseptic conditions, each monkey was implanted with a cylinder for microelectrode recording, and fitted with a head holder that allowed the head to be fixed in the standard stereotaxic position during the experiment. Scleral search coils were implanted to measure eye movements (Judge, Richmond, & Chu, 1980). The configuration of the experiment is shown in Figure 1.

Figure 1

The monkeys faced a translucent tangent screen (85 x 85[deg] at a distance of 235 [mm]), on which moving random-dot patterns were back-projected via the galvanometer

mirror system. The visual stimulus started to move at 10 - 160 [deg/s] in a preferred direction or an anti-preferred direction, 50 - 250 [ms] after the end of a centering saccade. Preferred direction here denotes the direction among eight directions (up, down, left, right, and intermediate directions between these four directions), in which each Purkinje-cell (P-cell) was activated most vigorously. Each visual stimulus ramp lasted 250 [ms] except in the altered stimulus duration conditions. In the altered stimulus duration condition, stimulus lasted 10 - 160 [ms]. An ocular following response (OFR) is induced by the motion of the whole field retinal image with shorter latency than that in smooth pursuit eye movements.

During the OFR, the mirror velocity, and the horizontal and vertical components of eye position and eye velocity, measured by the search coils and filtered by a 6-pole analog Bessel filter (100 [Hz]), were recorded at 500 [Hz]. The speed of the random dot pattern on the screen was in proportion to the mirror velocity. The single P-cell simple spike activity of VPFL discriminated by a time-amplitude window discriminator was simultaneously recorded at 1000 [Hz].

2.2 Data preparation

To analyze the relation between the VPFL P-cell firing frequency and eye movement, the P-cell firing and eye movement data of many trials (14-317 trials, average±SD = 95.5±36.9) under the same stimulus conditions for each P-cell were ensemble averaged after excluding the trials with saccadic intrusion. The responses were aligned with the stimulus onset (TIME 0), and the eye acceleration profiles were obtained by digital differentiation of eye velocity profiles after the averaging. The ensemble average firing pattern (i.e., firing frequency temporal pattern) was further low-pass filtered by a 6-pole Bessel digital filter with the same cut-off frequency (100 Hz) as that of the analog filter for the eye movements, since the different filtering for firing frequency and eye movement causes parameter estimation error (Slotine & Li, 1991). The positive direction of eye position, velocity, and acceleration was taken as the preferred direction of each neuron. Table 1 shows experimental conditions of 232 data sets from 30 P-cells whose preferred direction were downward.

Figure 2 shows typical simple-spike activity of a P-cell in the left VPFL together with eye angular acceleration, velocity, and position during the OFR to a 40 [deg/s] downward test ramp movement of a large random dot pattern (ensemble average of 194 trials). The firing frequency of this neuron became significantly different from the baseline rate 51 [ms] after the onset of stimulus motion. In the data shown, the eyes began moving several milliseconds

after the onset of the neural responses.

Table 1

Figure 2

2.3 Analysis method

(1) P-cell firing reconstruction

Natural eye movements are not driven by a single neuron but are driven by many neurons in several regions. It is therefore impossible in principle to make a causal model of the relation between the firing pattern of a single neuron and eye movements. To analyze the relation between eye movements and neural activity, we instead used an inverse-dynamics representation that could reconstruct temporal patterns of ensemble average firing frequencies of P-cells. The representation is based on the following equation:

$$\hat{f}(t-\delta) = M\ddot{\theta}(t) + B\dot{\theta}(t) + K\theta(t) + f_{bias}, \qquad (1)$$

where, $\hat{f}(t)$, $\ddot{\theta}(t)$, $\dot{\theta}(t)$, $\theta(t)$, δ, and f_{bias} are respectively the reconstructed firing frequency at time t; the eye acceleration, velocity, position at time t; the time-lag between the firing frequency and the movement; and the bias term. Note that the bias term dose not directly indicates the spontaneous firing level because it could contain the positional bias term, hence it could be estimated as negative value. The four coefficients M, B, K, f_{bias} and the time-lag δ were estimated to minimize the squared error between the observed and the reconstructed

firing frequencies (i.e., $f(t)$ and $\hat{f}(t)$, respectively) shown in Equation 2.

$$E(\delta, M, B, K, f_{bias}) = \sum_{t} \left(\hat{f}(t) - f(t) \right)^2 \qquad -20 \le \delta \le 20 \text{ [ms]} \qquad (2)$$

This minimization is nonlinear problem because the time-lag should also be estimated. Several local minima could exist on this cost function (Equation 2), which would disturb the search for the minimal error solution. To avoid missing optimal solution in this nonlinear minimization problem, a linear regression method was applied to estimate M, B, K, and f_{bias} at each δ (every one millisecond) within the limited time range. The plausible transmission time from a P-cell firing to an eye-ball movement can be estimated about 9 [ms] (Lisberger, 1988) or 8.6-10.9 [ms] (Shidara & Kawano, 1993). Thus the search area for estimation of time-lag, δ was thus limited from -20 to 20 [ms].

(2) Modeling check and data classification for reliable parameter estimation

The regression method described above could be used for any data sets and could derive some parameters even if reconstructions were unsuccessful. To guarantee the reliability of estimated parameters when the model is defined (i.e., Equation 1), data sets whose estimated coefficients are not reliable should be excluded. There are three possible causes for unreliable estimation: First, the model is not suitable for describing the relation between the P-cell firing pattern and the movement. In this case, the reconstructed firing frequency would not well fit the observed firing frequency, and the fitting error would show some trends. Second, the P-cell firing and/or eye movement were insufficiently modulated by the visual stimulation. Third, the number of trials was not enough to represent the firing frequency pattern. In this case, the sampling noise would be more remarkable than the signal. The second and third causes above would greatly affect the signal to noise ratio. It is not economical to apply the boundary limit independently for the modulation level of P-cell activity and the number of trials of these data sets, because both the firing pattern of well modulated P-cell with small number of trials and that of little modulated P-cell with many trials could be successfully reconstructed. Then some indexes should be required to classify the many data into three groups: data unsuitable for the applied model, data inappropriate for the parameter estimation, and data appropriate for the parameter estimation. We here applied following four methods to classify the data sets for reliable parameter estimation. The first two methods are to find data sets unsuitable for the defined model. From two different points of view, these methods

focus on the modeling errors which mainly depend on the number of averaging trials. The other two methods are mainly for keeping the reliability of estimated parameters.

Binominal distribution test

For testing each regression result, the first method evaluates the regression error depending on the ensemble averaged number of trials in each data set. Let us imagine two firing patterns whose fitting indexes, *coefficient of determination* values (explained below), are almost same, but one firing pattern is represented by averaging with few trials and the other similarly modulated is by averaging many trials. It should be regarded that the regression with few trials is more successful than that with many trials because the averaged data from few trials would be contaminated by sampling noise more than that from many trials. And it should be suspected that the firing pattern with many trials contains other factors which are not included in the model. To obtain accurate estimation results, ensemble averaged data with many trials should be more available than that with few trials. In experiments, however, the recording period of the neural activity was limited by experimental condition, thus number of trials was limited differently for each neuron. To evaluate the fitness of modeling in each ensemble averaged data set from different number of trials, the number of trials in each condition should be take into account for the fitness evaluation. It might be reasonable to assume that the firing spike at time t occurs with the 'ideal firing probability' at time t, $p(t)$, which would be obtained by ensemble averaging a huge number of trials under a single condition. The number of observed spikes at time t in n trials, $x(t)$, varies because of sampling noise and might therefore differ from $p(t) \cdot n$ when the number of trials is limited. This kind of phenomenon could be modeled by a binominal distribution, so the cumulative distribution function with *correction for continuity* of binominal distribution is calculated by

$$Q(x(t)|n, p(t)) = \sum_{i=0}^{x} \binom{n}{i} p^i (1-p)^{n-i} - \frac{1}{2}\binom{n}{i} p^x (1-p)^{n-x}. \qquad (3)$$

When the number of trials, n, is sufficient or $p(t)$ is sufficiently excited, the distribution of $Q(x(t)|n, p(t))$ for all t in ensemble averaged data will be uniform. We checked the firing reconstruction reliability under this presupposition as follows. First, we assumed that the reconstructed firing frequency at time t, $\hat{f}(t)$, is the 'ideal firing probability' , $p(t)$. Then we could compute $Q(x(t)|n, \hat{f}(t))$ in each time step under a single condition by substituting $\hat{f}(t)$

for $p(t)$. The observed spike number, $x(t)$, was calculated by $f_{nf}(t-t_f)\cdot n$ in which f_{nf} denotes the non-filtered firing frequency, t_f compensates the time delay caused by the filter (in this case, $t_f = 2[ms]$), and n denotes the trial number. If the reconstructed firing frequency, $\hat{f}(t)$, is, over time, appropriate as proper 'ideal firing probability', $p(t)$, the distribution of Q will be close to uniform distribution under the presupposition mentioned above. Then, we checked the difference between the experimental distribution of Q of each data set and the uniform distribution by Kolmogorov-Smirnov test for evaluating the goodness of modeling.

Auto-correlation test

In the above test method, it is assumed that no other noise except sampling noise caused by the limitation of the number of trials. In the actual experiment, however, it would be possible for observed firing frequency to be contaminated by other noise, such as fluctuation of the probability of firing in every trial. The actual noise variance will thus be larger than that expected by binominal distributions, and the distribution of Q, calculated under the assumption of binominal distribution, would not be close to the uniform distribution. We therefore prepared another 'soft' check method for taking care of modeling error. The second method focused on the residual error of the regression, which itself should not be correlated when the model was appropriate to represent the firing frequency. To avoid the filtering effect for residuals, we checked normalized auto-correlation coefficients of the differences between the non-filtered firing frequencies, $f_{nf}(t-t_f)$, and reconstructed firing frequencies, $\hat{f}(t)$, as shown in the equation

$$C(\tau) = \frac{E_t[e(t)\cdot e(t+\tau)]}{\sqrt{E_t[e(t)^2]\cdot E_t[e(t+\tau)^2]}}. \qquad (4)$$

Here, $E_t[\cdot]$ denotes the averaging in time t, and $e(t)$ denotes the difference between $f_{nf}(t-t_f)$ and $\hat{f}(t)$. If $e(t)$ can be regarded as random, this auto-correlation function, $C(\tau)$, will be close to zero at all τ except $\tau = 0$. We checked those values for each data set.

Coefficient of determination test (CD test)

Third, a performance index "*coefficient of determination*" (Hines & Montgomery, 1972)

expressed in Equation 5 was evaluated to select the data sets which could be well reconstructed by a simple linear model (i.e., Equation 1).

$$R^2 = 1 - \left(\sum_t \left(\hat{f}(t) - f(t) \right)^2 \Big/ \sum_t \left(f(t) - \overline{f} \right)^2 \right) \tag{5}$$

Here, $\hat{f}(t)$ is the reconstructed P-cell firing frequency and $f(t)$ denotes the observed firing frequency pattern. $\overline{f}$ is the temporal averaged firing frequency, that is constant over time. The index, *coefficient of determination*, takes the range $0 \leq R^2 \leq 1$, and comes close to 1 when the reconstructed firing frequency is close to the observed one. If the firing frequency is not linearly correlated with the eye acceleration, velocity and position, this index comes close to 0, hence the estimated parameters should be less reliable. This index equals the *correlation coefficient* squared.

Time-lag test

In the fourth method, we applied a time-lag test to guarantee the reliability of the estimated time-lag δ. In the analysis procedure described above, the *coefficient of determination* was obtained for δ at one-millisecond intervals from -20 to 20 [ms]. The curve of the relation between the time-lag and the *coefficient of determination* should be convex near the maximum point in each data set if time-lag is reliably estimated. To quantitatively evaluate this characteristic, the relation between the time-lag and the *coefficient of determination* for each data set was shifted independently in both axes so that the maximum point of the *coefficient of determination* becomes the origin (i.e., zero point). This procedure is expressed by Equations 6 and 7, and illustrated in Figure 3 (a)-(c). The relation between the time-lag and the *coefficient of determination* of *i*-th P-cell, Ψ_i, which is obtained numerically, is expressed as

$$CD = \Psi_i(TL). \tag{6}$$

Here, *CD* and *TL* respectively denote the *coefficient of determination* and time-lag. Let us replace *CD* and *TL* with *rCD* and *rTL* (relative *coefficient of determination* and relative time-lag) as shown in the next equations to normalize for the relation between *CD* and *TL* in each data sets. $CD_{\max}$ denotes the maximum *coefficient of determination* in the limited

range, $-20 \le \delta \le 20$ [ms], and TL_{max} denotes the time-lag at the maximum *coefficient of determination.*

$$rCD = CD - CD_{max}$$
$$rTL = TL - TL_{max} \qquad (7)$$

To illustrate this method, Figure 3(a) shows the original relation curves of three data sets (maximum point of each curve is indicated as '+'), and Figure 3(b) shows the relation curves of them after shifting. Figure 3(c) is the magnified view of Figure3(b) near the axes origin. In each graph, dot marks indicate the points obtained by regression. If the value of *coefficient of determination* is insensitive to change in time-lag, the relation curve is not sharp convex at the maximum point, the estimated time-lag (i.e., maximum point of *coefficient of determination*) is not reliable. The change in *coefficient of determination* around the maximum point of the line No.3 in Figure3(a) is not sharp compared to those of the lines indicated as No.1 and No.2, indicating the estimated time-lag and other parameters of No.3 were less reliable. To exclude these insufficient data sets for parameter estimation, the 'accept window' (±6[ms], -0.003) was used (thick bar in Figure 3(c)). The data sets whose relation curves did not cross in the plus and minus range of the accept-window bar were excluded from the estimated parameter analyses. The relation curve of excluded data (No.3) is indicated as dotted line in Figure 3(b)(c).

Figure 3

---

(3) Appropriate model checked by Cp-statistics

As mentioned in the previous section, insufficient models for fitting can cause unsuccessful modeling. By using the first two methods described above, we can check whether or not the data are suitable for the prepared model, but these methods do not address

the suitability of the model representation for the data sets. To examine this problem, we applied t-test for the estimated coefficients and checked Cp-statistics of several linear models. The procedure to select a suitable model by using Cp-statistics is described below. We checked three models: (a) a velocity, position, and bias model with time-lag, (b) an acceleration, velocity, position, and bias model with time-lag, and (c) a jerk, acceleration, velocity, position, and bias model with time-lag. Cp-statistics is expressed as follows.

$$Cp = \frac{\sum_{t}\left(\hat{f}(t) - f(t)\right)^2}{\hat{\sigma}^2} - n + 2p. \qquad (8)$$

Here, n is the number of data for the regression, p is the number of degrees of freedom for the model, $\hat{\sigma}^2$ is the estimated population variance, $\hat{f}(t)$ is the estimated firing frequency and $f(t)$ is the observed firing frequency. In this analysis we used the estimated variance of the full term model (c) (Hines & Montgomery, 1972) as the estimated population variance, $\hat{\sigma}^2$. The Cp-statistics of each model was calculated for each data set to confirm the best model for the firing frequency reconstruction and parameter estimation among these three models.

3. Results

3.1 Reconstruction of Purkinje-cell firing pattern

Here, we demonstrate the P-cell firing reconstruction by the inverse dynamics representation (i.e., Equation 1). To examine the local relation between the P-cell activity and eye movement in each condition, the reconstructed firing patterns under each stimulus condition are shown as **local fitting** in subsection 3.1(1). And to examine the global relation between them, the reconstructions of multi-condition data sets by one parameter set are demonstrated as **global fitting** in subsection 3.1 (2). The multi-condition data sets were obtained by combining several data sets taken under different stimulus conditions.

(1) Local fitting

Figure 4(a) shows an observed firing frequency pattern (dotted line, the same data as in Figure 2) and a reconstructed P-cell firing frequency pattern (thick line) from the eye movement

by using the estimated coefficients, M, B, K and time-lag, δ. In this case, the estimation error was minimal at a time-lag of 7 [ms]. The *coefficient of determination* was 0.93, indicating that the simple linear inverse-dynamics representation can satisfactorily predict complex time courses of P-cell firing. Figure 4(b) shows the temporal patterns of components decomposed into the acceleration, velocity, position, and bias terms of Equation 1. As shown in this figure, although the acceleration coefficient (M) was small (0.0621 [(spikes/s) / (deg/s^2)]), its component $M\ddot{\theta}(t)$ was predominant in the initial phase of the response, and its velocity component $B\dot{\theta}(t)$ was dominant in most of the rest. After the initial phase, the acceleration component decreased and the position component $K\theta(t)$ increased. The position component, however, had a reversed sign of the direction of the movements. Figure 5 shows the other reconstructed firing frequencies of: (a) a preferred direction stimulation (80[deg/s]), (b) an anti-preferred direction stimulation (-80[deg/s]), and (c) a shorter duration stimulation (20 [ms]) . In the case (a), reconstructed firing frequency pattern looked close to the observed firing frequency, but the *coefficient of determination* was not so high (CD=0.64, δ=10[ms]) because of the sampling noise caused by small number of averaging trials (23). In the case (b), the stimulus moved opposite to the preferred direction, and the firing frequency was decreased from the spontaneous firing level. Because of the high spontaneous firing frequency of P-cell (about 80 [spike/s] in this case), this firing pattern could be well decoded by the eye movement (CD = 0.85, δ=11[ms]). In the case (c), the P-cell firing was quickly decayed because the stimulus was eliminated by mechanical shutter 20 [ms] after the onset of stimulus velocity. The firing pattern was different from the former two cases, but was also well reconstructed by the eye movement (CD = 0.74, δ=8 [ms]) as well as they were in the preferred and anti-preferred direction stimulus conditions.

Figure 4

Figure 5

---

(2) Global fitting

We here introduce reconstructions of firing frequency patterns taken under multiple conditions of a single P-cell by one parameter set. Figure 6 shows, from top to bottom row, stimulus velocity patterns, observed single P-cell firing frequency patterns (gray line) superimposed by the reconstructed one (solid line), eye acceleration patterns, eye velocity patterns, and eye position patterns under 5 different stimulus velocities in the preferred direction. The P-cell firing frequency patterns were reconstructed by one parameter set for all 5 stimulus conditions, and were in good agreement with the observed firing frequency patterns in all conditions. The *coefficient of determination* was 0.84, indicating that the simple linear inverse-dynamics representation could satisfactorily predict complex time courses of P-cell firing in the case of global fitting as well as local fitting. The estimation error was minimal when the time-lag was 8 [ms], and the estimated acceleration, velocity, and position coefficients were respectively 0.108 [(spike/s)/(deg/sec^2)], 2.92 [(spike/s)/(deg/sec)], and -23.0 [(spike/s)/deg]. The upper graphs in Figure 7(a) show the stimulus velocities in the anti-preferred direction, and the lower graphs show the observed firing frequencies (gray line) and the reconstructed firing frequencies (solid line). Figure 7(b) shows those in the duration change condition in the same manner. The *coefficients of determination* were respectively 0.75 and 0.78. These successful reconstructions by one parameter set indicate that the activities of these P-cells almost linearly contributed to ocular following eye movements under several conditions.

Figure 6

Figure 7

3.2 Local data analysis

By statistically analyzing reconstruction results of many VPFL P-cells under several conditions, we examine the role of VPFL in the cerebellum for the ocular following eye movement. As mentioned in 2.3 (2), three major causes could lead to unsuccessful reconstruction: (1) the regression model is insufficient, (2) observed signal is not sufficiently

modulated, and (3) the number of trials is too small to represent the firing frequency pattern. The estimated parameters obtained by these unsuccessful reconstructions should not be used for examining averaged behavior of VPFL P-cells. In 3.2 (1), we examine whether or not the inverse dynamics representation (i.e., Equation 1) is suitable. Moreover, we classify all of the data sets into suitable data group and unsuitable one for reliable parameter estimation. In (2), we describe estimated parameters of Equation 1 (i.e., M, B, K, f_{bias}, and δ) and the distribution of them, and explain the trends of estimated coefficients in different stimulus conditions. In (3), we perform the reliabilities of estimated coefficients by confidence interval. In (4), we examine a sufficiency of the inverse dynamics representation by two statistical methods, t-test and Cp-statistics.

(1) Modeling check and data classification

Binominal distribution test

In accordance with the methods described in 2.3 (2), we first show the results of analysis based on the binominal distribution of firing spikes. Figure 8 shows the relation between the mean squared error of modeling (Equation 2) and the averaging number of trials. Each '+' is obtained from each data set. The curve indicates the firing variance predicted by the binominal distribution model using the mean firing frequency of all data sets. The modeling error tended to decrease as the number of trials increased. This is because the sampling noise that would contribute to a large fitting error depended greatly on the number of averaging trials. Thus we could not check the performance of modeling only by the mean squared error. We therefore calculated the cumulative distribution function given by Equation 3 for each data set. Figure 9 (a) shows the cumulative distribution functions of Q in Equation 3 for successful data sets classified by Kolmogorov-Smirnov test (significance level = 0.02) for uniform distribution whose theoretical cumulative distribution function is straight line (indicated as a white line in the same figure), and (b) for unsuccessful data sets. The large number of successful data sets (175/232) indicates that the model in appropriate to analyze the firing frequencies. However, 57 data sets were classified into unsuccessful data group. Figure 10 shows one sample of the reconstructed firing pattern of unsuccessful data with observed firing frequency. The observed firing frequency was relatively smooth because of the large number of averaging trials (148). The *coefficient of determination* was therefore relatively high, even though the reconstructed firing pattern does not look close to the observed one. By using the binominal distribution test method, the data sets like this unsuccessful sample could be excluded. All of the number of successful and unsuccessful data sets under different

stimulus condition are shown in the last part of this subsection.

Figure 8

Figure 9

Figure 10

Auto-correlation test

As mentioned in 2.3(2), the strict condition was assumed in the above test method. Next, we applied 'soft' test method, auto-correlation test. Figure 11 shows auto-correlation functions of the difference between the non-filtered firing frequencies, $f_{nf}(t-t_f)$, and reconstructed firing frequencies, $\hat{f}(t)$. The data whose auto-correlation function calculated by Equation 4 crossed the threshold ±0.25 over 10 [ms] of τ, was regarded as unsuccessful in this test. The auto-correlation functions of all successful data sets (208/232) are superimposed in Figure 11(a), and those of all unsuccessful data sets (24/232) are superimposed in Figure 11(b). The large number of successful data sets indicates that the model could describe the firing frequencies in most case. The number of successful data sets by this test was larger than that by the binominal distribution test, mainly because there is no precondition about the noise distribution function (or firing probability distribution function) in this test. By using this test, data set shown in Figure 10 was classified into unsuccessful data sets as in the binominal distribution test.

Figure 11

Coefficient of determination test

Figure 12 shows the histogram and the quantile box plot of the *coefficient of determination* (CD) for 208 data sets accepted by the auto-correlation test. The data sets whose CD was greater than 0.6, were 70.2 % of these data sets (146/208). Note that the CD could easily be affected by noise components, and the signal-to-noise ratio of the firing frequency in each data set depends on several factors, such as the number of averaging number, the dynamic range of the P-cell firing frequency, the dynamic range of the eye movement, and the magnitude of stimulus velocity. To find the reason for the low CD, we plotted in Figure 13(a)-(d) the relation between CD and several indexes: averaging number of trials, mean of squared firing frequency (subtracted spontaneous firing level), mean of squared eye acceleration, and stimulus velocity. Each plus mark denotes the relation of each data set in these figures. The correlation coefficient values between CD and these indexes are indicated above each graph. As clearly shown by these values, the CD was correlated more closely with the mean of squared firing frequency than with the other indexes, indicating that the low CD was due to the weak modulation of those P-cells under any stimulus conditions.

Figure 12

Figure 13

Time-lag test

Figure 14(a) shows the relations between time-lag (TL) and *coefficient of determination* (CD) for all of the data sets (146) chosen by above tests (i.e., auto-correlation test, and $0.6 \leq R^2$). The shifted relations between the time-lag and the CD for these sets are superimposed in Figure 14(b). The horizontal axis represents the relative time-lag (rTL), and the vertical axis represents the relative CD (rCD). To exclude the data sets whose CD was insensitive to change in time-lag, δ, the accept-window (±6[msec], -0.003) indicated in Figure 14(c) was used. The 37 data sets, whose rCD did not decrease more than 0.003 at ±6[ms] and were

excluded from the analyses of coefficients described below.

Figure 14

All test results are summarized in Table 2. Numbers in 4rd-7th columns indicate the number of the data sets selected by each test. Right two columns show the number of the data sets chosen by '**strict selection condition**' (combination of the binominal distribution test, the CD test, and the time-lag test) and by '**loose selection condition**' (combination of the auto-correlation test, the CD test, and the time-lag test). As shown in the right two columns, the number of the successful data sets depended on the stimulus conditions. Note that under the condition of preferred direction, 160 [deg/s] stimulus, only a few data sets were accepted. This might be due to nonlinearities rather than the weak activation of firing frequency. The details are discussed later. As mentioned in the 2.3 (2), firing frequency pattern could be contaminated by noises other than sampling noise, the most of numbers of successful data sets of loose selection condition were larger than those of strict selection condition. In the proceeding sections, the estimated parameters of the 109 data sets chosen by the **loose selection condition** were mainly analyzed.

Table 2

---

(2) Estimated latency and coefficients

The histogram and the quantile box plot of estimated time-lags of selected data sets (109) are shown in Figure 15. The mean time-lag was 7.47 [ms] (4.23 S.D.). In 54.1 % of the selected data sets (59/109), the estimated time-lag was between 8 and 11 [ms], which was very close to the latency elicited by electrical stimulation (8.6-10.9 [ms]) (Shidara & Kawano, 1993). This satisfies the prerequisite for the firing frequency to represent the motor command. On the other hand, there were some extreme values which cannot be explained reasonably by a known transmission time between P-cell activity and eye movement. Those CD values

were not so high ($0.6 \leq R^2 \leq 0.66$), thus it is possible that three check methods failed to exclude them as unsuccessful data sets. However, positive large time-lag potentially caused by longer tract from P-cell to eye movement, and negative large time-lag by feedback or efference copy signal of the eye movement. Clarifying these aspects needs further experiments.

The histograms and quantile box plots of estimated coefficients of acceleration, velocity and position, and of bias for selected data sets (109) are shown in Figure 16. The plots of the estimated coefficients had single peaks and had few extreme values. Table 3.1 summarizes the means and standard deviation values of the coefficients for 109 data sets (loose selection condition) and for 89 data sets (strict selection condition). The variances of the coefficients and time-lag were not large, so the P-cell firing frequency patterns in VPFL were roughly similar to each other during the ocular following response and the typical firing pattern of P-cell could be characterized by averaged coefficients. As shown in Table 3.2, however, these values were slightly different in three different conditions, stimulus in preferred direction, stimulus in anti-preferred direction, and change in stimulus duration. The magnitude of coefficients of acceleration, velocity, and position during the stimulus in the preferred direction were larger than those in the anti-preferred direction, indicating that the eye movements in the preferred direction were less sensitive for the P-cell activities. To compare the sensitivities in the preferred and the anti-preferred direction, the coefficients of 7 P-cells under the stimulus speeds of 40 and -40 [deg/s] were compared in Figure 17(a)-(c). This figure clearly shows that the magnitude of the most of coefficient of 40 [deg/s] speed stimulus condition were larger than those of -40 [deg/s]. This kind of difference also found in different kind of eye movement (vestibulo-ocular reflex) by Lisberger et al. (1994). To show the details of the difference in each stimulus speed, the coefficient values of accepted data sets are plotted against stimulus speed in Figure 18(a)-(c). Each line merges the estimated coefficients for each P-cell under several speeds. As shown in Figure 18(b)(c), the magnitude of coefficients of velocity and position tended to be small as the stimulus velocity increased in positive directions. In the negative directions, this trend was weaker, though found in several P-cells. For the acceleration, the coefficients in negative direction were smaller than those in positive direction, and there was no general trends in the positive direction. In summary, firing frequencies in local condition were successfully reconstructed by linear model, but the coefficients of some P-cells were slightly different in each condition, indicating nonlinear relation under global conditions of those P-cells existed between P-cell activity and eye movement.

Figure 15

Figure 16

Table 3.1

Table 3.2

Figure 17

Figure 18

---

(3) Reliability of estimated coefficients

We here check the reliability of estimated coefficients by a statistical index, confidence interval (Hines & Montgomery, 1972). Figure 19 shows the histograms of 95 % confidence intervals for estimated acceleration, velocity and position coefficients, and a bias. The means and standard deviations of the confidence interval for the coefficients and bias (M, B, K, f_{bias}) were respectively 0.0225 [(spike/s)/(deg/s^2)] ($\pm$0.00833 S.D.), 0.610 [(spike/s)/(deg/s)] ($\pm$ 0.230 S.D.), 5.23 [(spike/s)/deg] ($\pm$1.93 S.D.), and 20.3 [spike/s] ($\pm$9.20 S.D.). The confidence interval of each estimated coefficient was several times smaller than the variance of each estimated coefficient, indicating that the average values of the estimated coefficients would not be greatly affected by the estimation ambiguity.

Figure 19

---

(4) Necessity and sufficiency of the second order model

In the above analyses, the model for firing reconstruction was defined in advance as a second order linear inverse dynamics representation. For further analyses, the representation of the model should be determined by the dynamics between P-cell outputs and eye movements. In this section, we examine the sufficiency of the model used here by using two statistical test methods: t-test and Cp-statistics.

In many of the previous studies on modeling and analyzing the relations between slow eye movements and the activity of eye motor neurons or related brain regions, first-order linear systems with a position term and a velocity term have been utilized. This might be because the inertia of the eyeball is negligibly small, and the frequency responses between the activity of eye motor neurons and the eye movements obtained experimentally could be well fitted by a first-order system with delay (Reinhart & Zuber, 1970), indicating that the coefficients of acceleration are small (Robinson, 1981).

On the other hand, Robinson (Robinson, 1965) proposed a high-order model from the viewpoint of mechanical properties of the eye system. Keller (1973) succeeded in explaining the eye motoneuron firing frequency by a second-order model that included an acceleration-dependent term. Fushs et al. (1988) pointed out the necessity of using higher-order terms to explain the different motoneuron firing frequencies of different motoneurons.

Recent studies have suggested that acceleration properties are encoded by the P-cell in the initial phase of slow eye movements (Stone & Lisberger, 1990). How can we determine the differential order suitable for analyzing the relations between neural activities and eye movements? To determine the appropriate differential order for the inverse dynamics representation, we checked the following third-order model having a jerk, an acceleration, a velocity, a position, and a bias term with time-lag:

$$\hat{f}(t-\delta) = J\dddot{\theta}(t) + M\ddot{\theta}(t) + B\dot{\theta}(t) + K\theta(t) + f_{bias}\ , \qquad (9)$$

Here $\hat{f}$ denotes the reconstructed firing frequency of the P-cell at $t-\delta$; f_{bias} denotes the bias; and J, M, B, and K respectively denote the jerk, acceleration, velocity, and positional coefficients.

First, the original 232 data sets analyzed in 3.1(1) were again analyzed by Equation 9 instead of Equation 1. Then, 113 appropriate data sets were selected by the loose selection condition. The necessity of each component on the right side of Equation 9 was examined by *t*-test for the null hypothesis in which the coefficient of each component is zero. The number of the data sets classified by *p*-values of the t-tests are listed in Table 4. In many cases (89/113) the null hypothesis for the jerk component was not rejected ($0.05 \leq p$). This result indicates that the jerk component is almost unnecessary for reconstructing the P-cell firing frequency patterns from eye movements. On the other hand, the small *p*-values for the other components (i.e., acceleration, velocity, positional, and bias components) indicate that these components are necessary for reconstruction.

Table 4

Further, we examined Cp-statistics values of all of data sets (232) using three models: (a) a velocity, position and bias model, (b) an acceleration, velocity, position and bias model, (c) a jerk, acceleration, velocity, position, and bias model. The Cp-statistics value was minimum for the model (b) in 72.4 % of the data sets (168/232). This result also indicates that the jerk term in the inverse model (Equation 7) is unnecessary for most data sets whereas the acceleration term is necessary.

3.3 Global data analysis

In the above analysis, linear regression was done separately for each single condition. As demonstrated in 3.1 (2), not only for local condition but also for global condition (multi-conditions), P-cell firing frequency pattern could be reconstructed by the inverse dynamics

representation with one parameter set although nonlinearity under the global condition in some P-cells was found in the local data analysis. We here statistically analyze reconstructions of firing frequency patterns taken under multiple conditions of each single P-cell by one parameter set. The firing patterns observed in a single P-cell were categorized into several groups by the stimulus conditions: (1) the preferred direction stimulus, (2) the anti-preferred direction stimulus, (3) the change in stimulus duration, (4) the preferred direction stimulus and anti-preferred direction stimulus, and (5) the preferred direction stimulus and change in stimulus duration. The second column in Table 5 shows the number of prepared data sets combined as multi-conditions in each group. The same selection methods used in the local data analysis were applied for them. The number of the data sets selected by the loose selection condition and by the strict selection condition are listed in the right two columns in Table 5. Because of the nonlinearity, especially at 160 [deg/s] as mentioned in the last part of local data analysis, and of small modulation induced by the stimulation of anti-preferred direction, the firing frequencies were properly reconstructed only in few data sets in any group. However, the average estimated coefficients and time-lags of the successful data sets for the three conditions (pref. dir., anti-pref. dir., duration) (Table 6) are similar to those estimated in the local analysis (Table 3.1).

Table 5

Table 6

3.4 The data sets excluded from the coefficient analyses

As shown in Table 2, the percentages of the data sets accepted by the loose selection in local fitting were small (< 50 %) under the slow speed stimulus conditions (-20, -10, 10 [deg/s]) and the high speed stimulus conditions (-160, 160 [deg/s]). For the global fitting, the

all of the number of data sets accepted by loose selection were small in all conditions. This subsection discusses possible reasons. Figure 20(a) shows the relations between the stimulus speed and the root mean squared firing frequency (spontaneous firing level was subtracted) of 21 P-cells for preferred stimulus direction (positive speed) and of 15 P-cells for anti-preferred stimulus direction (negative speed). As shown in this figure, the P-cell firing under the slow speed stimulus conditions were little modulated. Therefore, the CD tended to be small as observed in Figure 13(b) hence the number of successful data sets in these conditions by the CD test was small as listed in 6th column of Table 2. As a result, the numbers of successful data sets by combination test (loose selection) for slow stimulus speeds were small.

Figure 20

On the other hand, the activities of P-cells were well modulated under the high speed stimulus conditions (both pref. and anti-pref. directions). The number of accepted data sets in the CD test under 160 [deg/s] speed condition (see 6th column in Table 2) is not small (17/21). The most of the data sets under the preferred direction condition in global fitting (see fifth column in Table 5) were also accepted (18/21), in which the firing frequencies were well excited by multi-conditions. Figure 21(a) is one sample of the unsuccessful data in the global fitting under the preferred direction stimulation condition. Upper graphs show the stimulus velocities and lower graphs show the observed and the reconstructed firing frequencies. The reconstructed firing frequency (gray line) did not fit well to the observed firing frequency (solid line). As observed by Shidara et al. (1993) and as shown in Figure 20(a), the firing frequencies were saturated at higher stimulus speed, indicating that there were some nonlinear factors between the stimulus speeds and the firing frequencies. To examine the linearity between the spike firing frequency and the eye movement, the relations between the root mean square of firing frequency and the root mean square of eye velocity of 21 P-cells under the preferred direction stimulus conditions (see Table 5) were drawn in Figure 20(b) and Figure 20(c). The dots indicate the data points under different speed conditions and the small circles indicate the data points for 160 [deg/s] stimulus speed. Figure 20(b) shows those relations for successful P-cells (9 set) in the global fitting listed in the most right column in Table 5 and Figure 20(c) shows those relations for the P-cells (12 set) excluded by the loose

selection in global fitting. Although the linear relations between the firing frequency and the eye velocity could be found in many P-cells between 10 - 80 [deg/s] both in successful and unsuccessful data sets, the points for 160 [deg/s] in unsuccessful data sets (circles in Figure 20(c)) came off the linear relations, which were on the linear relation in (b). These nonlinear properties of the excluded data sets could cause poor fitting for the data set under the high speed stimulus conditions in the local fitting and also for the data sets in the global fitting. In addition, estimated coefficients of local fitting were slightly different in each local condition. These nonlinear factors made it difficult to reconstruct the firing frequency in global fitting of many P-cells. We think they might be caused by the other driving signals from the other brain regions and/or the nonlinearity in the downstream neural processing.

In the global fitting, the percentages of the accepted data sets for the anti-preferred direction and for change in stimulus duration were also small (respectively, 20% (3/15) and 33% (2/6)) as well as that for the preferred direction condition. For the former condition, the number of the data sets accepted by the CD test was small (5/15) because the modulations of firing for anti-preferred direction were relatively small as shown in Figure 20(a). For example, though the firing in Figure 21(b) looks close to the observed firing frequency, this was excluded by the CD test. For the stimulus duration change condition, the number of the data sets accepted by the time-lag test was small (3/6). Since these two tests work not only for checking the fitting performance but also for keeping the reliability of estimated parameters, the small number of the data sets accepted by the loose selection dose not always mean poor fitting.

Figure 21

---

4. Discussion

4.1 Inverse dynamics representation versus forward dynamics representation

Several researchers have analyzed the relations between neural firing frequencies in some brain regions and some kinds of eye movements – such as saccade, fixation, and smooth pursuit (Fuchs & Luschei, 1970; Fuchs et al., 1988; Robinson, 1970), vergence (Keller, 1973; Keller & Robinson, 1972), and nictitating reflex (Berthier, Barto, & Moore, 1991) – by explicitly or implicitly assuming a causal forward dynamics representation. Reinhart & Zuber (1970) identified the transfer function from the oculomotor neuron to eye movement with a 1st order model with time-lag in the frequency domain. Berthier and his colleagues (1991) described the transfer function from firing responses in deep cerebellar neurons to nictitating membrane responses by using a causal moving average model in the time domain and several-order models in the frequency domain.

As pointed out in 3.3 (1), however, eye movements are driven not by a single neuron but by many neurons. Many signals from various brain regions converge finally into the eye motor neuron pool of the extraocular muscles, and these motor neurons discharge to generate muscle forces and do so in a manner independent of the type of movement (e.g., saccade or vergence) (Robinson, 1970). Motor neuron pools are the only regions which send motor commands directly to eye muscles. This is why a causal modeling (i.e., causal time domain analysis, causal frequency domain analysis) could be used to study the relationship between the firing frequency of eye motoneurons and eye movements. It is impossible in principle, however, to causally reconstruct eye movements from a single neuron activity in a particular higher brain region such as VPFL. There are two reasons for this: (1) some neurons may be concerned with some particular type of eye movement while some others may not be, (2) there may be several different motor centers affecting eye movements simultaneously.

The inverse-dynamics representation (Equation 1) seems similar to the forward-dynamics representation that predicts the movement from the motor command (neural activities), but is very different from and actually opposite to it in terms of the direction of information flow (Barto, 1989; Kawato & Gomi, 1992). For simplicity, let us assume Equation 10 as a causal system in which eye movement θ is driven by eye motor neuron firing f_m and that eye motor neuron firing is caused by Purkinje cell firing f_i and firing in other brain regions f_{rk}:

$$M_m\ddot{\theta}(t)+B_m\dot{\theta}(t)+K_m\theta(t)=f_m(t-\delta_m)=\sum_i w_i f_i(t-\delta_i)+\sum_k r_k f_{rk}(t-\delta_{rk}). \qquad (10)$$

Here, M_m, B_m, and K_m respectively denote the acceleration, velocity, and positional coefficients

with respect to eye motor neuron firing f_m, and w_i and r_k are respectively weights for firing frequencies of P-cells and those of neurons in other related brain regions. Eye movements $\ddot{\theta}(t),\dot{\theta}(t)$, and $\theta(t)$, cannot be reconstructed by a part of the inputs, f_i. One of the inputs, f_i, however, can be reconstructed by eye movements $\ddot{\theta}(t),\dot{\theta}(t)$, and $\theta(t)$. Furthermore, in the inverse-dynamics representation, any or all coefficients (M,B,K) of a single P-cell can be negative when the activities of other cells or regions compensate negative terms to get final stable total inputs. Unstable coefficient sets obtained by inverse modeling can not be used to reconstruct eye movements. Thus, the forward-dynamics representation, which requires all causal inputs, can be used only for the final common path (Robinson & Keller, 1972), hence it should not be used for P-cells.

4.2 Comparing the proposed method with previous methods

There are several previous studies about the quantitative relations between the firing frequencies in extra-ocular motor neurons and eye movements (Fuchs & Luschei, 1970; Fuchs et al., 1988; Keller, 1973; Keller & Robinson, 1972; Robinson, 1970). In these studies, they used various kinds of eye movements in which a particular motion component such as a position component or velocity component dominated. Miles et al. (1980), and Stone and Lisberger (1990) studied the relations between the P-cell firing frequencies at the VPFL and eye velocities during smooth pursuit movements for periodic targets.

Although these studies were remarkable in adopting quantitative methods to reveal the correlation between firing frequency and eye movement, there are limitations to their methods. First, they did not simultaneously decompose the firing frequency into position, velocity, and acceleration components. This could be the source of inaccuracy in decoding the firing frequency into each component, thereby leading to inaccurate value of estimated coefficient. Second, their sensitivity analysis for each component was independently carried out for different kinds of movements in which a particular component dominated. This method, however, is not effective if the characteristics of a neural activity are not the same for different types of movements. For the motor neuron, the relations between eye movements and neural activities are known to be consistent over any type of movement, as shown by Robinson et al. (1970) and Fuchs et al. (1970; 1988), so this method should be acceptable. In other higher brain regions, however, the contribution of a neural activity to movement might depend on the type of movement. Actually, it has been reported that many P-cells in the VPFL are not activated or are less activated for saccadic eye movements (Miles & Fuller,

1975), and that some P-cells in VPFL are modulated only in relation to saccade, interrupting their maintained discharge (Miles et al., 1980).

On the other hand, the proposed method in this paper can overcome these two limitations by applying simultaneous decomposition (i.e., multi-variable regression) to 'sufficiently rich' or 'persistently excited' (Sastry & Bodson, 1989) movements. The coefficients can be obtained from one particular kind of movement, and the reliability of estimation can be confirmed by checking the *confidence interval* of estimated parameters. Furthermore, we used eye movements under several conditions during OFRs which contained vast range of frequency, and we took ensemble averages of P-cell firing over trials under each identical condition to attain high-resolution. The difference between an observed firing frequency pattern and a reconstructed one could be reliably confirmed, and the dependency on each component could be examined by decomposition.

4.3 Comparing the obtained coefficients with those in previous reports

Miles et al. (1980) and Stone & Lisberger (1990) reported the firing frequency sensitivities of 'gaze-velocity P-cell' in VPFL with respect to the eye velocity during smooth pursuit eye movements. The mean value was 1.02 [(spike/s)/(deg/s)] (range: 0.21-2.86, ipsi) in Miles et al. (1980) and 1.34 [(spike/s)/(deg/s)] (down), or 0.99 [(spike/s)/(deg/s)] (ipsi) in Stone (1990). These values are two or three times smaller than the eye-velocity sensitivity (i.e., velocity coefficient) obtained in our analysis. The eye-position sensitivity during maintained fixation reported by (Miles et al., 1980) was very small (0.26 (0.87 max) [(spike/s)/deg] (ipsi), 0.17 (0.62 max) [(spike/s)/deg] (contra)), while the position coefficients in our analysis were not small (see results).

One possible reason for such differences is that P-cells contribute to the different type of eye movements in different ways. Another possible reason is the different methods to estimate parameter (sensitivity). The velocity-sensitivities in previous studies were obtained by comparing the peak-to-peak gains of firing frequencies and eye velocities. In Stone & Lisberger (1990), the phase shift of P-cell firing with respect to the eye velocity during periodic sinusoidal smooth pursuit eye movement (0.5 [Hz]) was 7 [deg] (that corresponds to 38.9 [ms]) (range -39 to 50 [deg]). In Miles et al.(1980), the range of phase shift of the gaze-velocity cells during smooth pursuit was between -53 and 59 [deg]. The forward phase shifts of P-cell firing, in particular, cannot be regarded as a pure time-lag between the firing and the eye movement because they should be about 9 [ms] if the neurons in question send

the motor commands for eye movements (Lisberger, 1988; Shidara & Kawano, 1993). Besides, there is no evidence that P-cell firing consists only of velocity-dependent component. The P-cell firing in their studies might contain other components (i.e., acceleration and/or position components) that were not taken into account when calculating the sensitivities. Though the positional component was subtracted based on the estimated value during fixation to obtain the velocity sensitivity in Miles et al. (1980), there is no guarantee that the position sensitivity of smooth pursuit is the same as that of fixation.

4.4 Cerebellum as a motor command generator

Several studies (Kawano et al., 1994; Kawano et al., 1992; Shidara, Kawano, Gomi, & Kawato, 1992) suggest that the neural firings in MST and DLPN encode the visual input signals and that the P-cells send the eye driving signals. Recent study (Takemura, Inoue, Gomi, Kawato, Shidara, & Kawano, 1994) have quantitatively shown the difference between the neural activity of MST/DLPN and that of VPFL. Miles (1980) and Stone & Lisberger (1990) suggested that the outputs of the Purkinje cells converged and/or diverge to interneurons in the brainstem which lead to the motor neurons. Figure 22 is a block diagram of the potential main pathway for generating the OFR (Kawano et al., 1994). It is interesting to know what part of the brain in this figure is mainly involved in generating motor commands for the OFR. We will discuss what signal is encoded by P-cells in the VPFL by comparing neuron activities downstream (motor neuron) and upstream (DLPN).

Figure 22

The connectivities from the VPFL P-cells to the motor neurons driving eye movements were confirmed by the electrical stimulation method in (Shidara & Kawano, 1993). Because the temporal averaged firing frequencies of P-cells differ from those of motor neurons, the coefficients obtained in each region cannot be compared directly. Rather we should compare the ratios of mean coefficients in both regions. The ratio of the mean acceleration coefficient

to the mean velocity coefficient ($E[M]/E[B]$) for the 109 data sets listed in Table 3.1 is 0.0251. This ratio is close to but slightly larger than that of extra-ocular motor neurons (0.015), calculated from the averaged time-constants of the 15 cases observed in (Keller, 1973). On the other hand, the ratio of the mean position coefficient to the mean velocity coefficient ($E[K]/E[B]$ = -4.42) for the P-cells was quite different from, and had the reversed sign to, that of motoneurons: 5.1. This result might indicate that the dynamic component of the movement is driven by the P-cells but the positional component of the movement (i.e., elastic term) is not positively driven by these P-cells. Two possibilities to interpret the negative position coefficients obtained by inverse modeling are the following:

(1) The VPFL send a negative position-related signal in order to compensate the excessive elastic component encoded by other brain regions in parallel with or downstream from the VPFL.

(2) A spurious correlation due to nonlinear transformation between neuronal firing and movement was extracted. If we assume that the velocity coefficient is large in the initial phase of the movements and gradually becomes smaller, linear analysis would lead to an estimation of too large velocity coefficient with a negative positional coefficient. This is because eye-position is gradually increased.

To give a more confident interpretation of negative coefficients for position terms, we need to analyze sufficiently modulated signals in both the upstream and downstream structures.

Consider now, the translation from DLPN outputs which are upstream of VPFL to eye motor commands. As shown by Kawano et al. (1992), the preferred directions in the DLPN were spread in all directions whereas those in the VPFL are only ipsilateral and downward (Shidara & Kawano, 1993). The firing temporal patterns are also different in each region: the acceleration component of the firing was more evident in the DLPN than in the VPFL quantitatively shown in (Takemura et al., 1994). This implies that the dynamic component of the final motor command is regulated by P-cells in VPFL, which supports the idea that the cerebellum is the main side of sensory-motor transformation.

From a comparison between P-cell activities and neural activities in upstream and downstream regions, we would like to stress that, at least in the VPFL, the cerebellum functions as a coordinated motor command generator rather than as a sensory information translator (Bower, 1992), even though some aspects of the motor command generator may be regarded as those of a sensory information translator. To examine the generality of the hypothesis: "cerebellum works as a motor command generator", it is necessary to quantitatively

analyze P-cell firing in many regions of the cerebellum during many kinds of movements.

4.5 Internal models of controlled objects for generating motor commands in the cerebellum

Given the cerebellar histological uniformity, several researchers have tried to understand the functional roles of the cerebellum for different type of motor control. The above considerations based on the previous and present studies have strongly suggested that some kind of sensory-motor command transformation is done in the cerebellum, but the details of functional mechanism in the cerebellum are still unclear.

Studies on smooth pursuit eye movements (Robinson, Gordon, & Gordon, 1986) and manual tracking tasks (Miall, Weir, & Stein, 1987) have revealed that these movements cannot be explained as simple feedback controllers because of the large delay in the nervous systems. Miall (1993) has therefore tried to explain the cerebellar function as a Smith predictor which predicts eye movements by using a forward dynamics model. At least in the VPFL, however, the P-cell output can be regarded as a motor command rather than an prediction of eye movement. To examine the computational function of the cerebellum needs the study to reveal what information is encoded in the inputs to the cerebellum.

Stone & Lisberger (1990) pointed out the importance of eye-velocity positive feedback to P-cells (carried by corollary discharge) rather than visual input (retinal error) after the initiation of pursuit. They showed the persistent firing of P-cells during smooth pursuit with no retinal error while the targets were stabilized on the fovea by servo controlled, and they concluded that sustained responses were driven by the eye-velocity inputs. The observation of Newsome (1988), Stone (1990), and Kawano (1994), however, are consistent with another possibility. When the visual target vanished for a brief period during smooth pursuit eye movement, the eye almost tracked the invisible target trajectory for a while (Stone & Lisberger, 1990) or slowed down slightly (Becker & Fuchs, 1985; Kawano et al., 1994). During this time, not only VPFL P-cells (Stone & Lisberger, 1990) but also MST neurons (Newsome et al., 1988; Sakata, Shibutani, & Kawano, 1983) continued firing or slowly decreased firing (Kawano et al., 1994) with no retinal slip signal. Thus, the MST output does not encode simple retinal slip signals; rather, they might encode a kind of desired or predicted eye movement. On the other hand, when the visual stimulus (random dot pattern) vanished during ocular following response, both the firing of the VPFL P-cell (cf. Figure 7(b)) and that

of the MST neuron (preliminary observation) decayed quickly, and the eye movement slowed down suddenly. These observations clearly indicate two points. First, the dominant signal for driving eye movement is some feedforward signals sent from the higher CNS upstream of VPFL rather than a feedback signal (like corollary discharge signals), not only during initiation but also during sustained movement. This must be so even if a kind of integrated signal (which could be supplied by corollary discharge to VPFL) might also be important as pointed out by Stone & Lisberger (1990) and as used in our ocular movement control scheme and simulations (Gomi & Kawato, 1992; Kawato & Gomi, 1992). Second, the input cannot be regarded as a simple discrepancy between a target and an eye movement because the firing is sustained when there is no retinal error during smooth pursuit with an invisible target (Newsome et al., 1988).

In summary, eye-driving-signals different from the motor commands could be sent to the P-cells from regions upstream of the cerebellum. If such eye-driving signals are related to the desired movements, the computational hypothesis that the cerebellum is a major site of the inverse dynamics model for controlled movement (Kawato, Furukawa, & Suzuki, 1987; Kawato & Gomi, 1992) would be encouraged as one of the main computational principles in cerebellum. Proving this hypothesis require the study to examine whether or not some inputs to the cerebellum are related to desired movements.

References

Barto, A. G. (1989). Connectionist learning for control. In T. Miller, R. S. Sutton, & P. J. Werbos (Eds.), *Neural Networks for Control* (pp. 5-58). MA: The MIT Press.

Becker, W., & Fuchs, A. F. (1985). Prediction in the oculomotor system: smooth pursuit during transient disappearance of a visual target. *Experimental Brain Research*, **57**, 562-575.

Berthier, N. E., Barto, A. G., & Moore, J. E. (1991). Linear systems analysis of the relationship between firing of deep cerebellar neurons and the classically conditioned nictitating membrane in rabbits. *Biological Cybernetics*, **65**, 99-105.

Bower, J. M. (1992). Is the cerebellum a motor control device? *Behavioral and Brain Sciences*, **15**(4), 741-742.

Fuchs, A. F., & Luschei, E. S. (1970). Firing patterns of abducens neurons of alert monkeys in relationship to horizontal eye movement. *Journal of Neurophysiology*, **33**, 382-392.

Fuchs, A. F., Scudder, C. A., & Kaneko, R. S. (1988). Discharge patterns and recruitment order of identified motoneurons and internuclear neurons in the monkey abducens nucleus. *Journal of Neurophysiology*, **60**(6), 1874-1895.

Gomi, H., & Kawato, M. (1992). Adaptive feedback control models of the vestibulocerebellum and spinocerebellum. *Biological Cybernetics*, **68/2**, 105-114.

Hines, W. W., & Montgomery, D. C. (1972). *Probability and Statistics in Engineering and Management Science, 3rd ed.* Wiley & Sons.

Ito, M. (1984). *The Cerebellum and Neural Control*. New York: Raven Press.

Judge, S. J., Richmond, B. J., & Chu, F. C. (1980). Implantation of magnetic search coils for measurement of eye position: an improved method. *Vision Research*, **20**, 535-538.

Kawano, K., Shidara, M., Watanabe, Y., & Yamane, S. (1994). Neural activity in cortical area MST of alert monkey during ocular following response. *Journal of Neurophysiology*, **71**, 2305-2324.

Kawano, K., Shidara, M., & Yamane, S. (1992). Neural activity in dorsolateral pontine nucleus of alert monkey during ocular following response. *Journal of Neurophysiology*, **67**, 680-703.

Kawato, M., Furukawa, K., & Suzuki, R. (1987). A hierarchical neural-network model for control and learning of voluntary movement. *Biological Cybernetics*, **57**, 169-185.

Kawato, M., & Gomi, H. (1992). The cerebellum and VOR/OKR Learning Models. *Trends in Neurosciences*, **15**(11), 445-453.

Keller, E. L. (1973). Accommodative vergence in the alert monkey motor unit analysis. *Vision Research*, **13**, 1565-1575.

Keller, E. L., & Robinson, D. A. (1972). Abducens unit behavior in the monkey during vergence movements. *Vision Research*, **12**, 369-382.

Lisberger, S. G. (1988). The neural basis for learning of simple motor skills. *Science*, **242**, 728-735.

Lisberger, S. G., & Fuchs, A. F. (1978). Role of primate flocculus during rapid behavioral

modification of vestibulo-ocular reflex. I. Purkinje cell activity during visually guided horizontal smooth pursuit eye movement and passive head rotation. *Journal of Neurophysiology*, **41**, 733-763.

Lisberger, S. G., Pavelko, T. A., Bronte-Stewart, H. M., & Stone, L. S. (1994). Neural basis for motor learning in the vestibuloocular reflex of primates. II. Changes in the responses of horizontal gaze velocity Purkinje Cells in the cerebellar flocculus and ventral paraflocculus. *Journal of Neurophysiology*, **72**(2), 954-973.

Miall, R. C., Weir, D. J., & Stein, J. F. (1987). Visuo-motor tracking during reversible inactivation of the cerebellum. *Experimental Brain Research*, **65**, 455-464.

Miall, R. C., Weir, D. J., Wolpert, D. M., & Stein, J. F. (1993). Is the cerebellum a Smith predictor? *Journal of Motor Behavior*, **25**(3), 203-216.

Miles, F. A., & Fuller, J. H. (1975). Visual tracking and the primate flocculus. *Science*, **189**, 1000-1002.

Miles, F. A., Fuller, J. H., Braitman, D. J., & Dow, B. M. (1980). Long-term adaptive changes in primate vestibuloocular reflex. III. Electrophysiological observations in flocculus of normal monkeys. *Journal of Neurophysiology*, **43**(5), 1437-1476.

Miles, F. A., Kawano, K., & Optican, L. M. (1986). Short-latency ocular following responses of monkey. I. Dependence on temporospatial properties of visual input. *Journal of Neurophysiology*, **56**(5), 1321-1354.

Newsome, W. T., Wurtz, R. H., & Komatsu, H. (1988). Relation of cortical areas MT and MST to pursuit eye movements. II. Differentiation of retinal from extraretinal inputs. *Journal of Neurophysiology*, **60**(2), 604-620.

Reinhart, R. J., & Zuber, B. L. (1970). Horizontal eye movements from abducens nerve stimulation in the cat. *IEEE Transactions in Biomedical Engineering*, **17**, 11-14.

Robinson, D. A. (1965). The mechanics of human smooth pursuit eye movement. *Journal of Physiology*, **180**, 569-591.

Robinson, D. A. (1970). Oculomotor unit behavior in the monkey. *Journal of Neurophysiology*, **33**, 393-404.

Robinson, D. A. (1981). Control of eye movements. In J. M. Brookhart & V. B. Mountcastle (Eds.), *HANDBOOK OF PHYSIOLOGY: SECTION 1 The Nervous System, vol.2 motor control, Part 2* (pp. 1275-1320). Maryland: American Physiological Society.

Robinson, D. A., Gordon, J. L., & Gordon, S. E. (1986). A model of the smooth pursuit eye movement system. *Biological Cybernetics*, **55**, 43-57.

Robinson, D. A., & Keller, E. L. (1972). The behavior of eye movement motoneurons in the arert monkey. *Biol. Ophthalmol.*, **82**, 7-16.

Sakata, H., Shibutani, H., & Kawano, K. (1983). Functional properties of visual tracking neurons in posterior parietal association cortex of the monkey. *Journal of Neurophysiology*, **49**, 1364-1380.

Sastry, S., & Bodson, M. (1989). *Adaptive Control.* NJ: Prentice Hall.

Shidara, M., & Kawano, K. (1993). Role of Purkinje cells in the ventral paraflocculus in short-latency ocular following responses. *Experimental Brain Research*, **93**, 185-195.

Shidara, M., Kawano, K., Gomi, H., & Kawato, M. (1992). Linear regression analysis of relationship between simple spike activity of purkije cells in the ventral paraflocculus of alert monkey and ocular following response. In *VIIIth TMIN International Symposium -Role of the Cerebellum and Basal Ganglia in Voluntary Movement-*, (pp. 70). Tokyo.

Shidara, M., Kawano, K., Gomi, H., & Kawato, M. (1993). Inverse dynamics model eye movement control by Purkinje cells in the cerebellum. *Nature*, **365**(2), 50-52.

Slotine, J. J. E., & Li, W. (1991). *Applied Nonlinear Control.* New Jersey : Prentice-Hall.

Stone, L. S., & Lisberger, S. G. (1990). Visual responses of Purkinje cells in the cerebellar flocculus during smooth pursuit eye movements in monkeys. I. Simple spikes. *Journal of Neurophysiology*, **63**(5), 1241-1261.

Takemura, A., Inoue, Y., Gomi, H., Kawato, M., Shidara, M., & Kawano, K. (1994). A linear regression time-series analysis of neural activity during ocular following. In *The 9th Symposium on Biological and Physiological Engineering*, (pp. 275-278). Tsukuba: SICE.

Captions

Figure 1. Configuration of the experiment.

Figure 2. Ensemble averaged patterns of 194 trials under the same stimulus condition (preferred direction stimulation 40 [deg/s]). From top to bottom: visual stimulus velocity, firing frequency of a single Purkinje cell, eye angular acceleration, eye angular velocity, and eye angular position.

Figure 3. Sample of the time-lag test. Relations between time-lag and *coefficient of determination* for the sample two data sets (a), and the shifted relations (b). The sampling points are indicated as small dots and the relation of each data set are merged by a line. In (a) the horizontal axis represents time-lag (*TL*) and the vertical axis represents *coefficient of determination* (*CD*). In (b) the horizontal axis represents relative time-lag (*rTL*), which denotes the difference from the maximum *TL* in each data set, and the vertical axis represents relative *coefficient of determination* (*rCD*), which denotes the difference from the maximum *CD* also in each data set. All operation to obtain these values are explained in Section 2.3. (c) shows the magnified view of (b) and accept window (thick solid line, (±6[msec], -0.003)) for selecting the data sets for which parameters could be properly estimated. Dashed lines denote the excluded case by this time-lag test, whose relation carve did not cross the accept window bar between 0 [ms] and 6 [ms].

Figure 4. (a) Reconstructed and observed VPFL P-cell firing patterns (preferred direction stimulation. 40 [deg/s]). (b) Components of reconstructed firing frequency ascribed to eye angular acceleration, angular velocity and angular position.

Figure 5. From upper to bottom: stimulus velocity, observed and constructed firing frequency, eye angular acceleration, angular velocity and angular position. (a) A preferred direction stimulation condition (-80[deg/s]) (b) An anti-preferred direction stimulation condition (-80[deg/s]). (c) a duration change stimulation condition (20 [ms])

Figure 6. From top to bottom row: stimulus velocity patterns, observed single P-cell firing frequency patterns (gray line), eye acceleration patterns, eye velocity patterns, and eye position patterns under 5 different stimulus velocities in the preferred direction. The reconstructed P-cell firing frequency patterns by one parameter set (i.e., global fitting) were superimposed in the graphs second row from the top (solid line).

Figure 7. The upper graphs in (a) (b) are the stimulus velocities in the anti-preferred direction, and the lower graphs are the observed firing frequencies (gray line) and the reconstructed firing frequencies (solid line) by one parameter set of the linear inverse model (i.e., global fitting). (a) anti-preferred direction stimulation conditions, (b) duration change stimulation conditions.

Figure 8. Mean squared error of modeling vs. the number of trials in each data set. Each '+' is obtained from each data set. The curve indicates the firing variance predicted by the binominal distribution model using the mean firing frequency of all data sets. The error of modeling tends to exponentially decrease as the number of trials increases.

Figure 9. Cumulative distribution functions of Q in equation (3), (a) for successful data sets deemed by Kolmogorov-Smirnov test (significance level = 0.02) for a uniform distribution whose theoretical cumulative distribution function is a straight line (white line), and (b) for unsuccessful data sets.

Figure 10. A sample of unsuccessful reconstruction classified by Kolmogorov-Smirnov test in the binominal distribution test.

Figure 11. Auto-correlation functions of the difference between the non-filtered firing frequencies, $f_{nf}(t-t_f)$, and reconstructed firing frequencies, $\hat{f}(t)$: (a) successful data sets ($-0.25 < C(\tau) < 0.25 \quad for \forall 10[ms] < \tau$), (b) unsuccessful data sets($C(\tau) \le -0.25 \mid 0.25 \le C(\tau) \quad for \exists 10[ms] < \tau$).

Figure 12. Histogram and quantile box plot of the *coefficient of determination* for all 208 data sets accepted by the auto-correlation test.

Figure 13. The relation between coefficients of determination and several indexes: (a) Trace number for ensemble averaging vs. *coefficient of determination* of each data set, (b) The variance of firing frequency vs. *coefficient of determination* of each data set, (c) The variance of the eye acceleration vs. *coefficient of determination* of each data set, (d) Stimulus velocity vs. *coefficient of determination* of each data set. Correlation coefficients between the *coefficients of determination* and those indexes are attached above each graph.

Figure 14. (a) Relations between *coefficients of determination* (*CD*) and time-lag (*TL*) for 146 data sets which were accepted by the auto-correlation test, and whose *coefficient of determination* at the maximum point was over 0.6. All relation curves of all data sets are superimposed. (b) Relations between relative *coefficient of determination* (*rCD*) and relative time-lag (*rTD*), for the same data sets. All operation to obtain these relation were described in Section 2.3. The relations of all case indicated as lines are superimposed in this graph. Solid lines denote the relation curves of the data sets accepted by the time-lag test, and dashed lines denote those of the rejected data sets. (c) Magnified view at the origin of (b) and the accept-window bar (±6[msec], -0.003).

Figure 15. Histogram and quantile box plot of estimated time-lags of 109 data sets accepted by the loose selection.

Figure 16. Histograms and quantile box plots of estimated coefficients of 109 data sets accepted by the loose selection. (a) acceleration coefficients, (b) velocity coefficients, (c) positional coefficients, (d) bias .

Figure 17. Comparison between estimated coefficients under a preferred and an anti-preferred direction stimulus conditions (-40 and 40 [deg/s]) of 7 P-cells. (a) acceleration coefficient, (b) velocity coefficient, (c) position coefficient.

Figure 18. Estimated coefficients of the accepted data sets under the speed conditions (95). Each line merges the estimated coefficients for single P-cell under several speed stimulations. (a) acceleration coefficient, (b) velocity coefficient, (c) position coefficient.

Figure 19. Distribution of the 95% confidence intervals for the estimated coefficients of 109 data sets. (a) acceleration coefficient (b) velocity coefficient, (c) position coefficient, (d) bias.

Figure 20. (a) The relations between the stimulus speed and the root mean squared firing frequency (spontaneous firing level was subtracted) of 21 P-cells for preferred stimulus direction (positive speed) and of 15 P-cells for anti-preferred stimulus direction (negative speed). Each line merges the data for single P-cell in different stimulus speeds. (b) The relations between the root mean square of firing frequency and the root mean square of eye velocity of 9 P-cells under the preferred direction stimulus conditions (see Table 5) which were accepted by the loose selection in global fitting. (c) shows those relations for the 12 P-cells excluded by the loose section in global fitting. In (b) and (c), the dots indicate the data points under different speed conditions and the small circles indicate the data points for 160 [deg/s] stimulus speed.

Figure 21. (a) one sample of the unsuccessful data in the global fitting under the preferred direction stimulation condition. Upper graphs show the stimulus velocities and lower graphs show the observed and the reconstructed firing frequencies. (b) one example of the data excluded by the *coefficient of determination* test in the same manner with (a).

Figure 22. Main pathway for generating ocular following eye movement

Table 1. Summary of the cell names and stimulus conditions of the prepared data sets. '@' in the column denotes the existence of data sets in all stimulus conditions as follows. In the 'preferred speed' condition, the random dot stimulus patterns were applied in 5 speeds, 10, 20, 40, 80, 160 [deg/s]. In the 'anti-pref. speed' condition, the stimulus speeds were changed in -10, -20, -40, -80, -160 [deg/s]. In the duration change condition, stimulus patterns were eliminated by a mechanical shutter , 10, 20, 40, 60, 80, 160 [ms] after the onset of stimulus movements of 80 [deg/s]. The number in the columns instead of '@' denotes the condition parameter, that is speed (unit [deg/s]) or duration (unit [ms]), of that neuron for which all stimulus patterns were not applied in the experiment.

Table 2. Summary of the tests for data sets under all stimulus conditions. In the second column, the number denotes the stimulus speed or stimulus duration, respectively. All the numbers of the data sets shown in 4th-7th columns indicate the number of the selected data sets by each test from all of the data sets prepared under each single stimulus condition (the number of data sets were indicated in third left column). Right two columns show the number of the data sets chosen by 'strict selection condition' (binominal distribution test, *coefficient of determination* test, and time-lag test), and by 'loose selection condition' (auto-correlation test, *coefficient of determination* test, and time-lag test). The number in the parentheses is the percentage of the selected data sets in those prepared for each condition.

Table 3.1. The average and standard deviation of estimated coefficients and time-lags of 109 data sets and of 89 data sets chosen by the loose selection condition and the strict selection condition, respectively.

Table 3.2. Summary of estimated coefficients and time-lag under three different stimulus conditions of 109 data sets chosen by the loose selection condition.

Table 4. Significance of each component of the reconstructed firing frequency. The *p*-values of *t*-test indicate the significance probability of the null hypothesis that the coefficient of

each component is zero. If the p-value is very small, the model fitting is performed poorly when that component is dropped.

Table 5. Summary of the tests for data sets in the four tests (the binominal distribution test, the auto-correlation test, the coefficient of determination test, and the time-lag test) and in the combined tests (the strict selection and the loose selection). The strict selection is the combination of three tests, the binominal distribution test, the coefficient of determination test, and the time-lag test. The loose selection is the combination of three tests, the auto-correlation test, the coefficient of determination test, and the time-lag test.

Table 6. Summary of averaged estimated coefficients and time-lag for the three conditions, preferred direction stimulus condition, anti-preferred stimulus condition, and stimulus duration change condition.

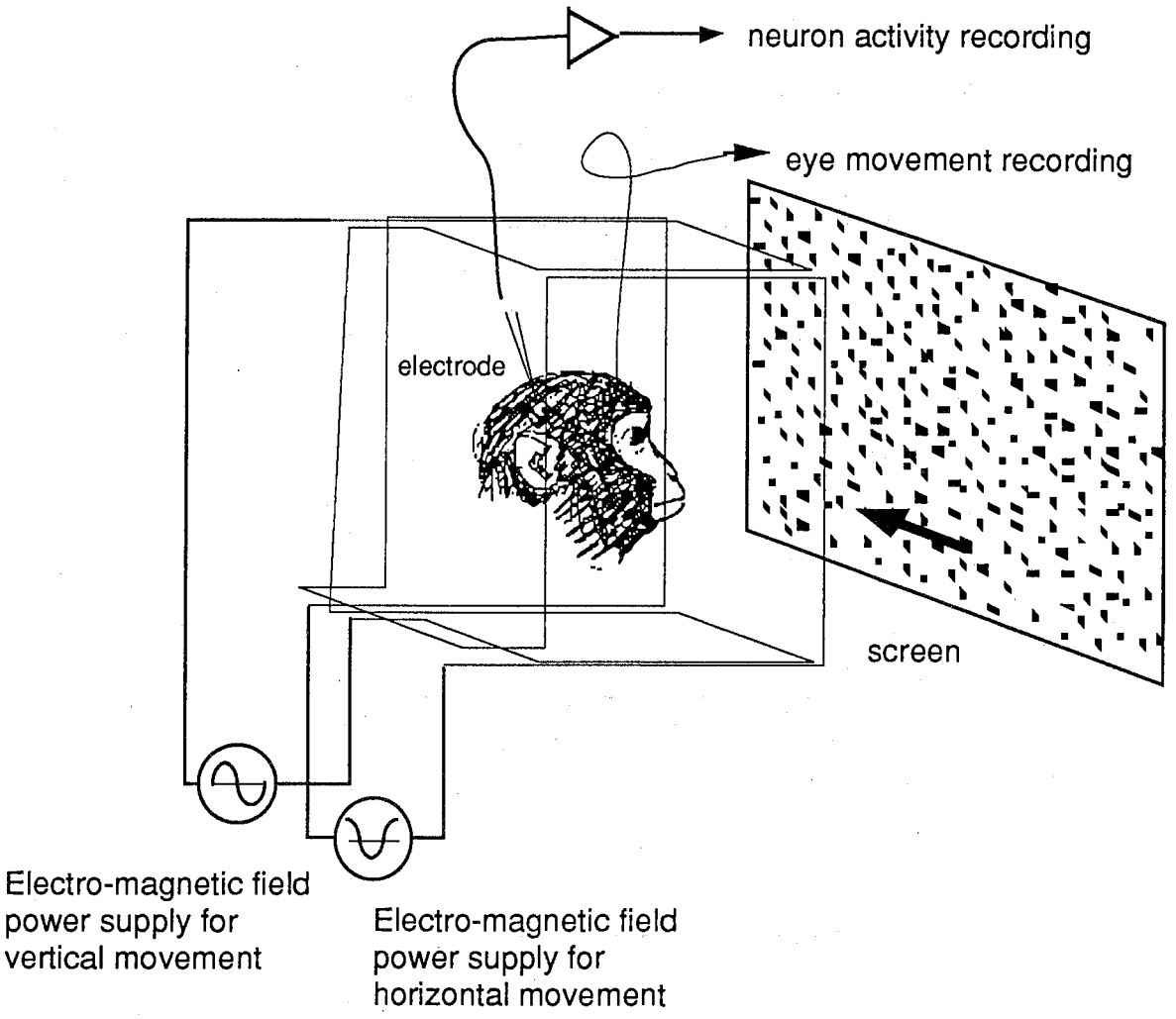
neuron activity recording
eye movement recording
electrode
screen
Electro-magnetic field
power supply for
vertical movement
Electro-magnetic field
power supply for
horizontal movement

Figure 1

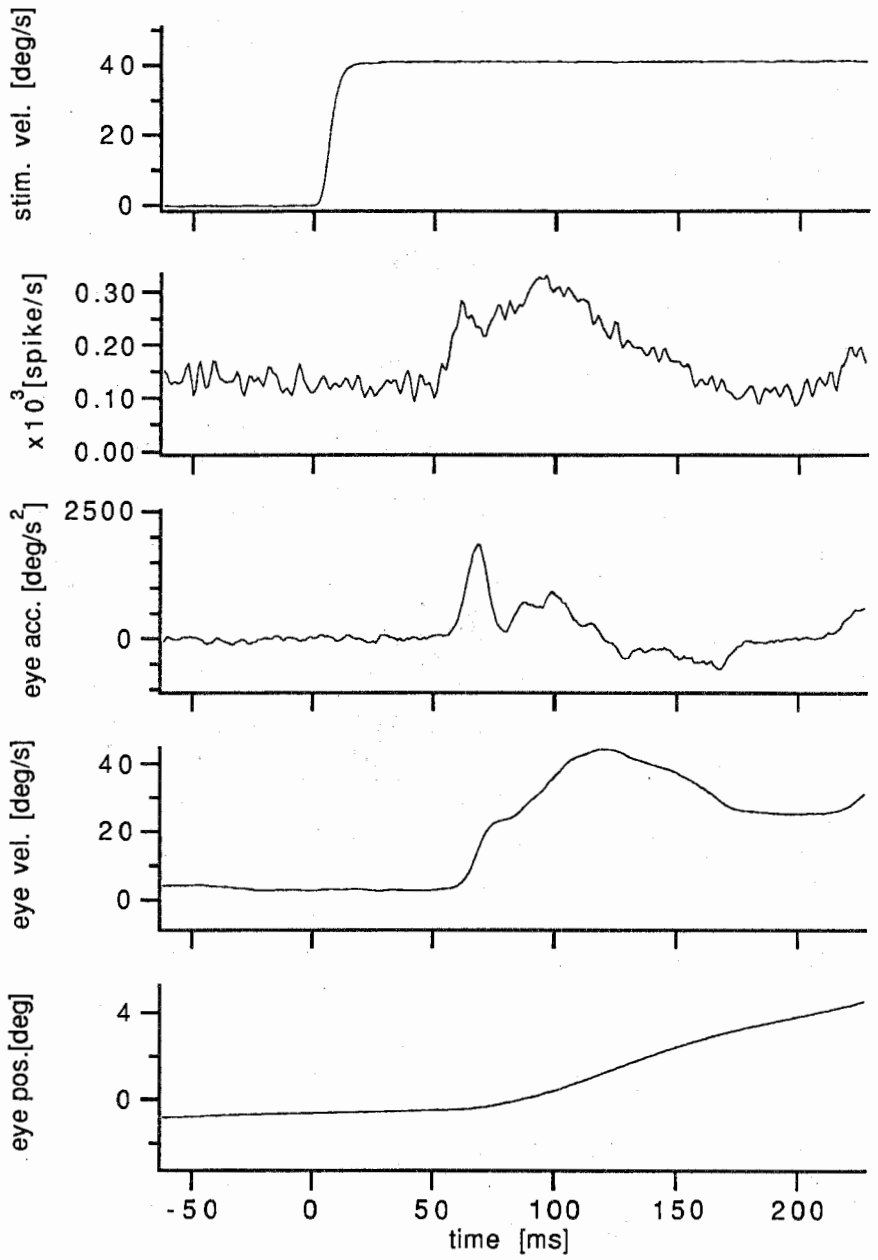
stim. vel. [deg/s]
40
20
0
x10^3[spike/s]
0.30
0.20
0.10
0.00
eye acc. [deg/s^2]
2500
0
eye vel. [deg/s]
40
20
0
eye pos.[deg]
4
0
-50
0
50
100
150
200
time [ms]

Figure 2

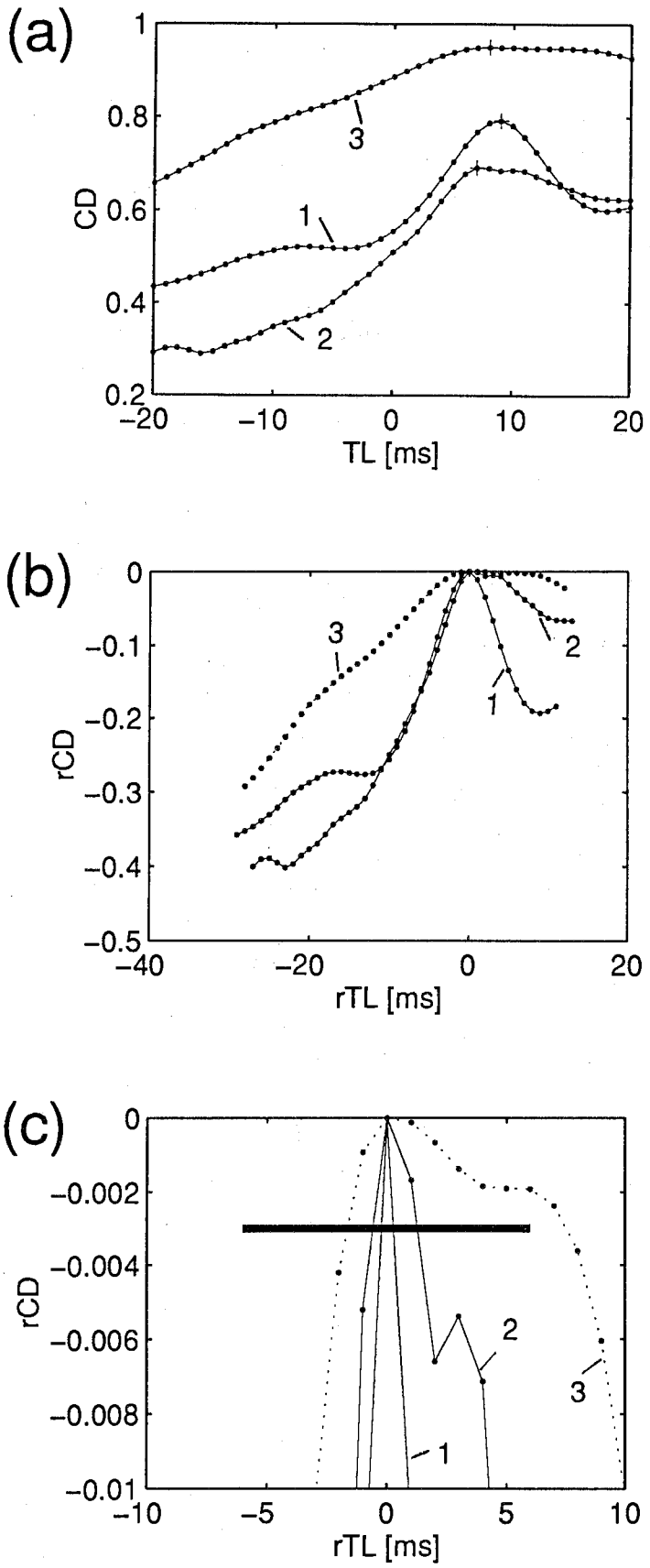

Figure 3

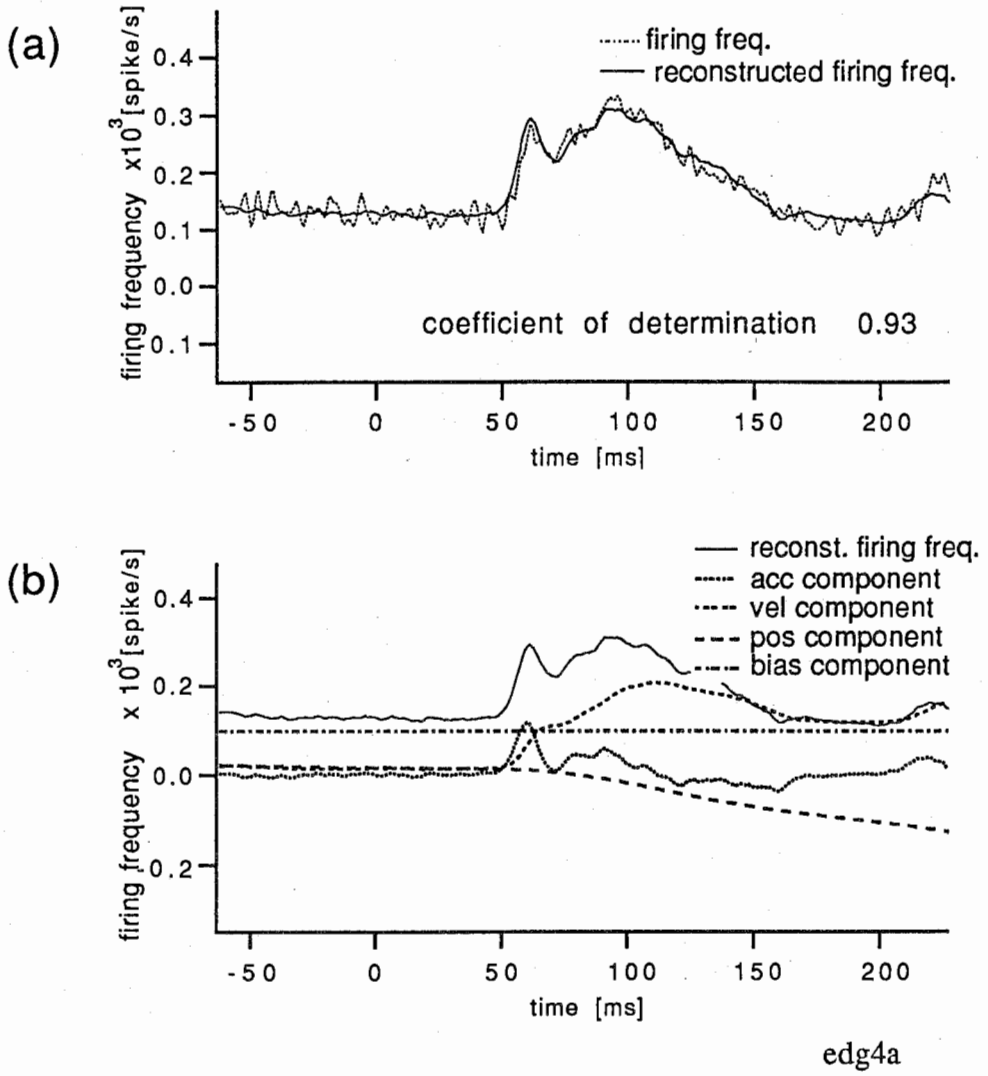
(a)
firing freq.
reconstructed firing freq.
firing frequency x10^3[spike/s]
0.4
0.3
0.2
0.1
0.0
0.1
coefficient of determination 0.93
-50
0
50
100
150
200
time [ms]
(b)
reconst. firing freq.
acc component
vel component
pos component
bias component
firing frequency x 10^3[spike/s]
0.4
0.2
0.0
0.2
-50
0
50
100
150
200
time [ms]
edg4a

Figure 4

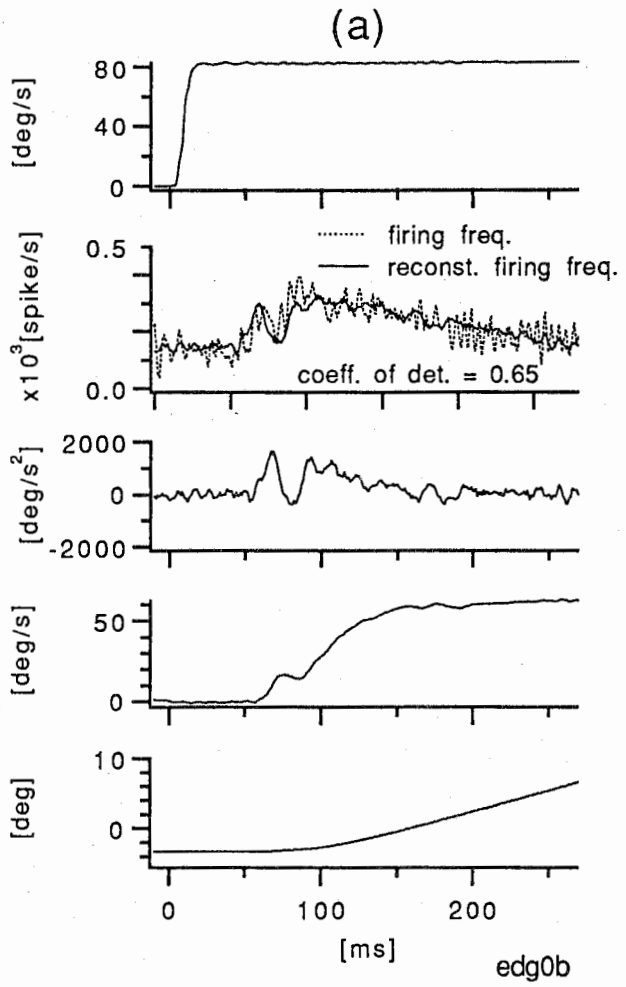
(a)
80
40
0
[deg/s]
0.5
0.0
x10^3[spike/s]
firing freq.
reconst. firing freq.
coeff. of det. = 0.65
2000
0
-2000
[deg/s^2]
50
0
[deg/s]
10
0
[deg]
0
100
200
[ms]
edg0b

Figure 5 (a)

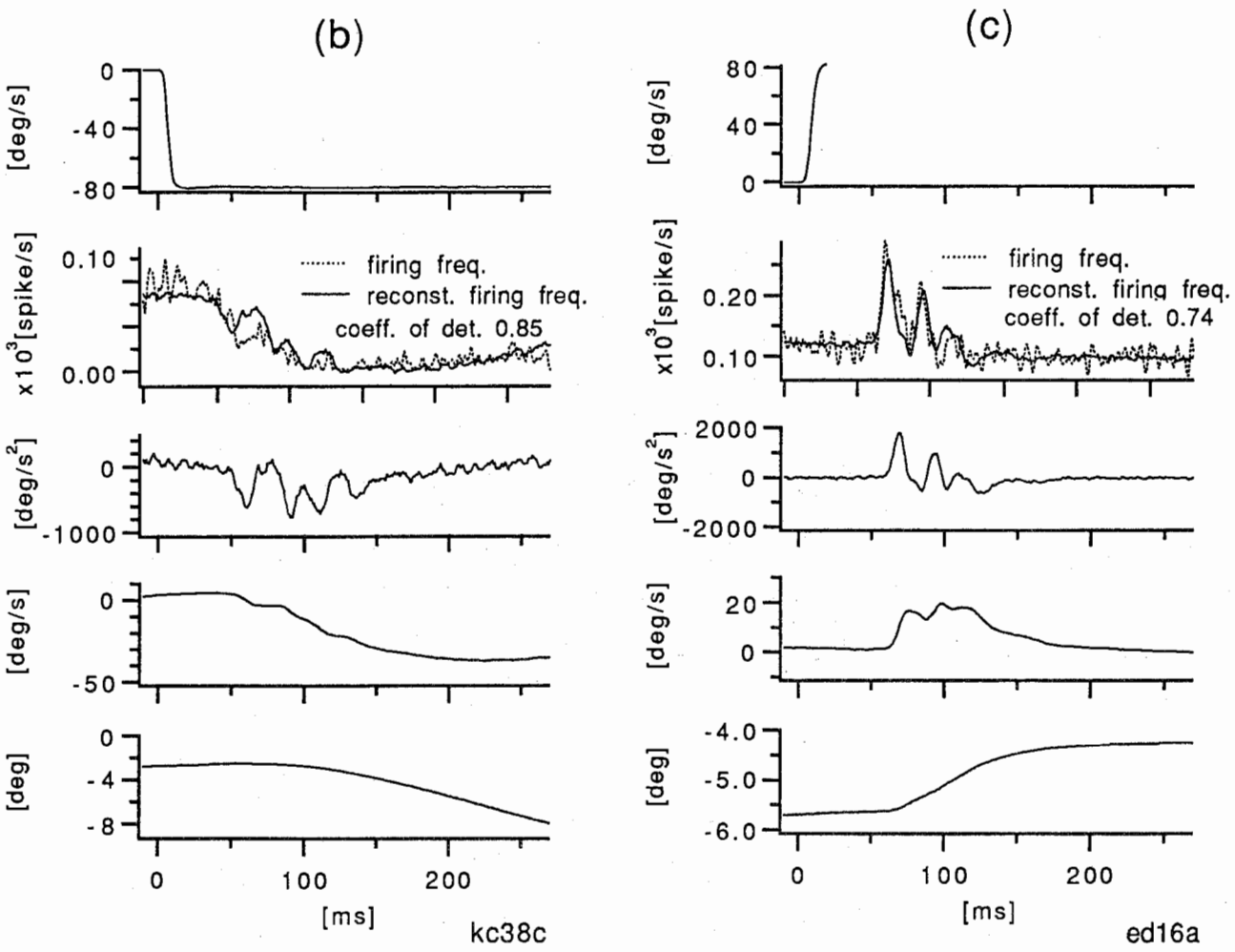
(b)
(c)
[deg/s]
0
-40
-80
80
40
0
x10^3[spike/s]
0.10
0.00
0.20
0.10
firing freq.
reconst. firing freq.
coeff. of det. 0.85
coeff. of det. 0.74
[deg/s^2]
0
-1000
2000
-2000
[deg/s]
0
-50
20
0
[deg]
0
-4
-8
-4.0
-5.0
-6.0
0
100
200
[ms]
kc38c
ed16a

Figure 5 (b), (c)

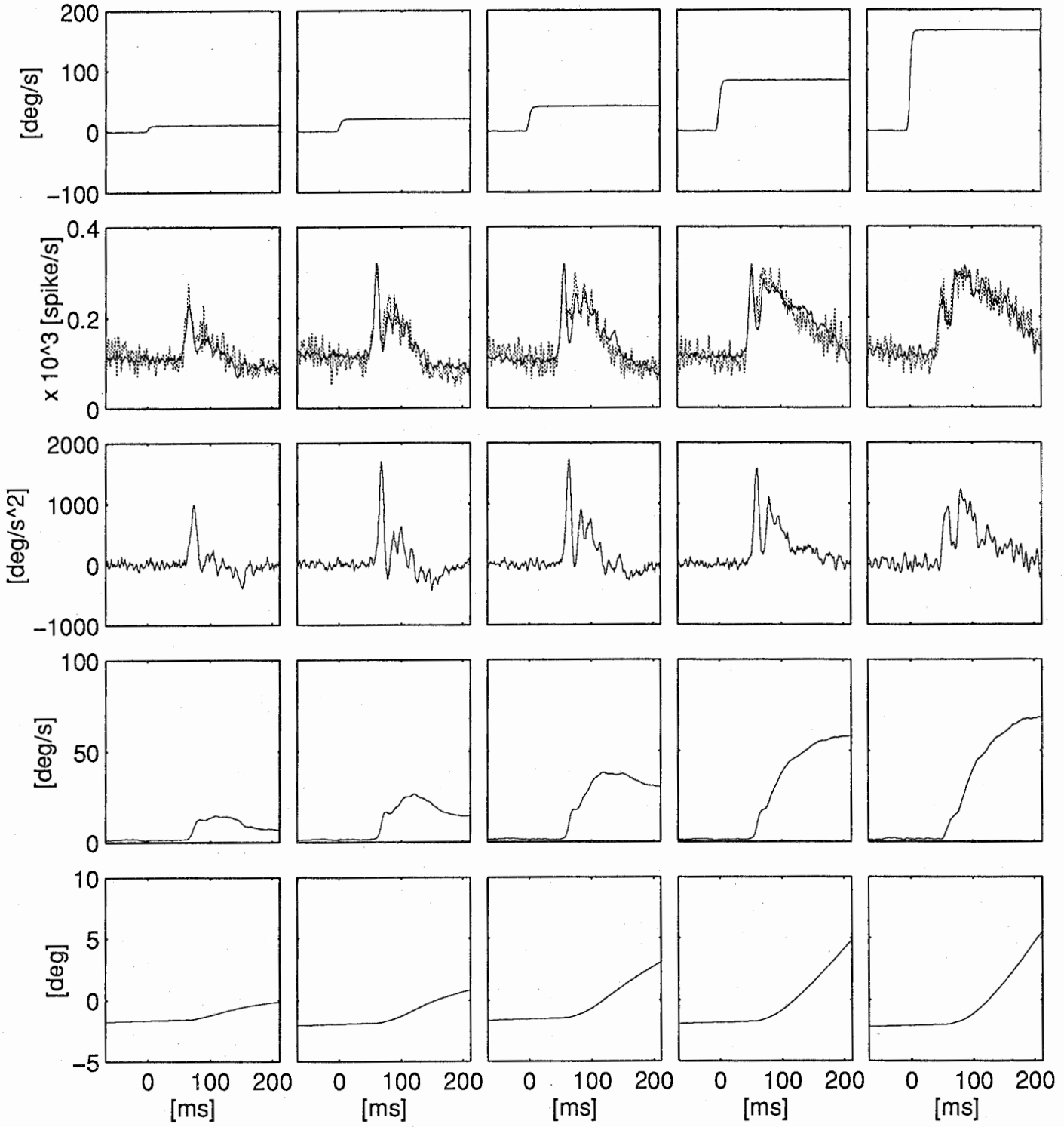
200
100
0
−100
[deg/s]
0.4
0.2
0
x 10^3 [spike/s]
2000
1000
0
−1000
[deg/s^2]
100
50
0
[deg/s]
10
5
0
−5
[deg]
0
100
200
[ms]

Figure 6

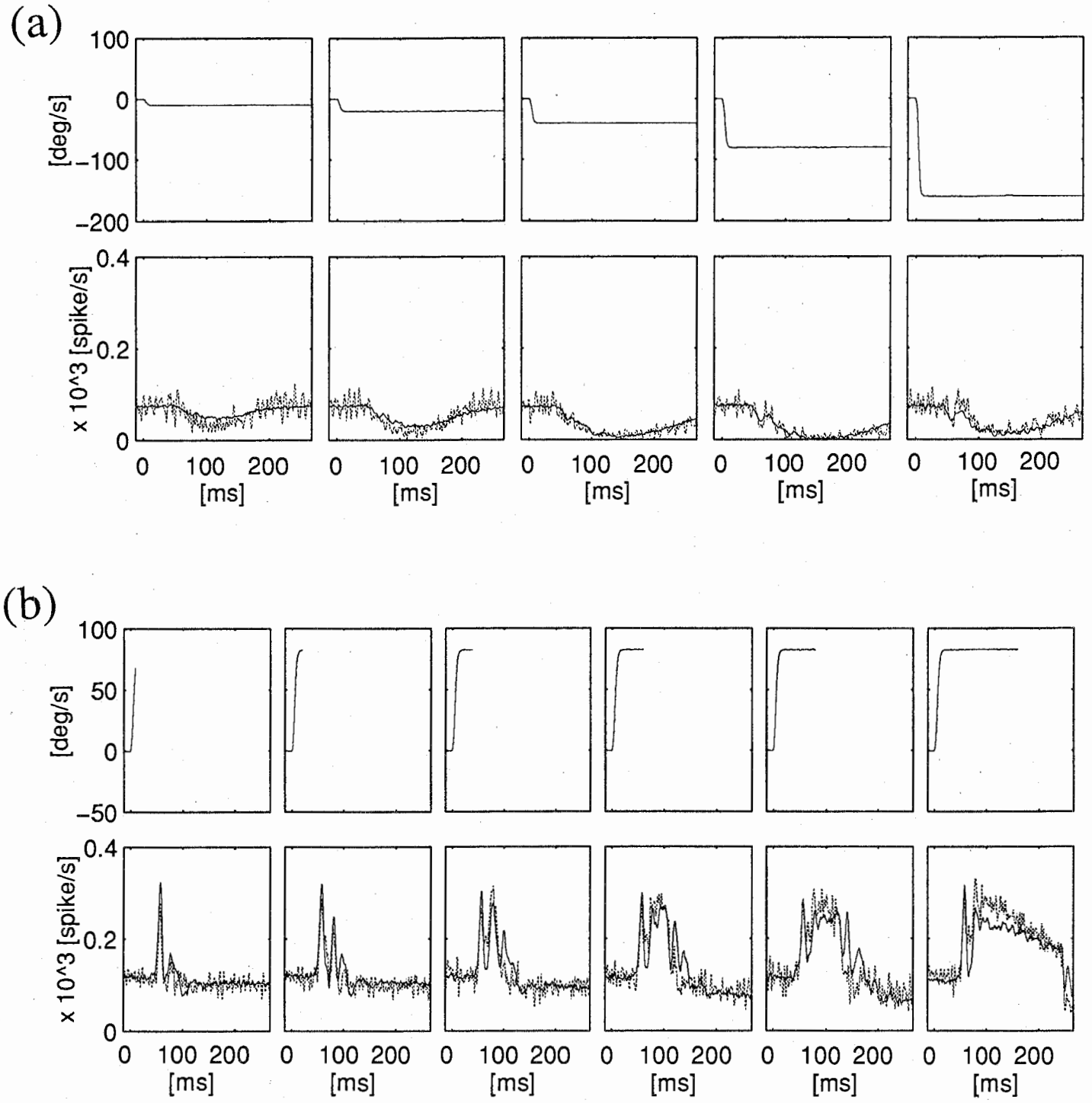
(a)
100
0
−100
−200
[deg/s]
0.4
0.2
0
x 10^3 [spike/s]
0 100 200
[ms]
(b)
100
50
0
−50
[deg/s]
0.4
0.2
0
x 10^3 [spike/s]
0 100 200
[ms]

Figure 7

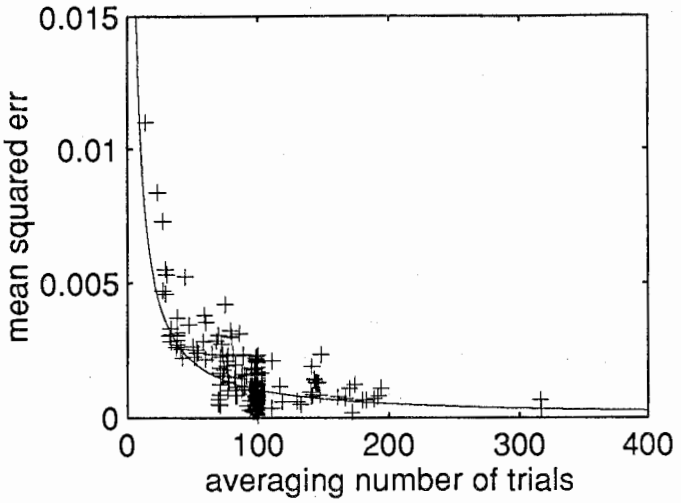

Figure 8

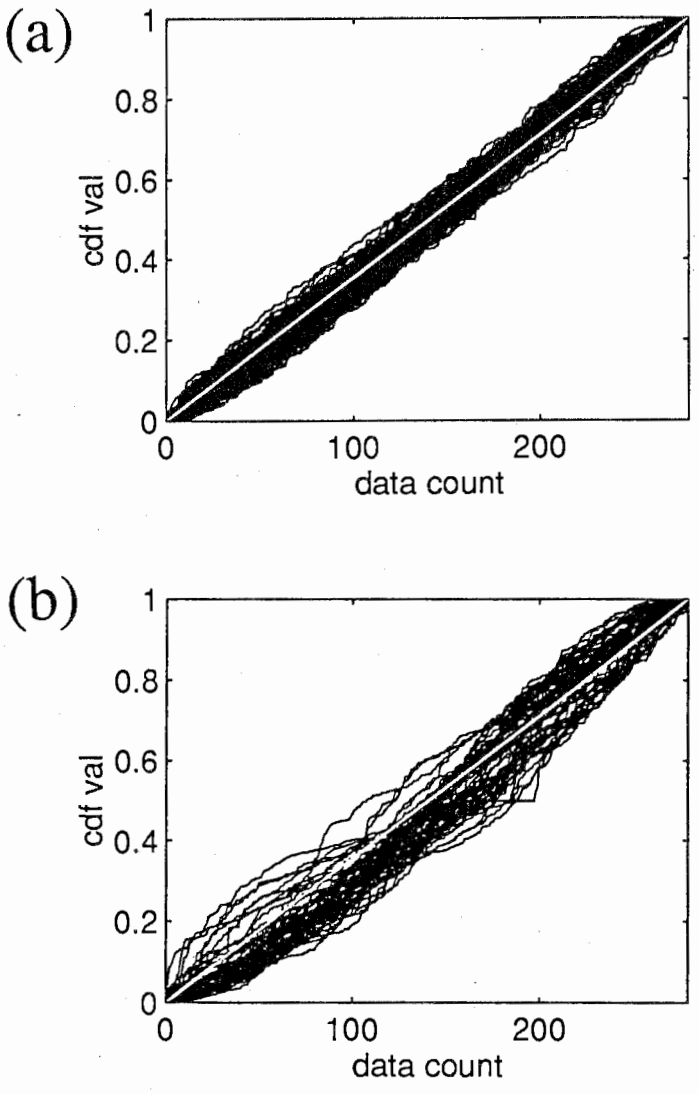

Figure 9

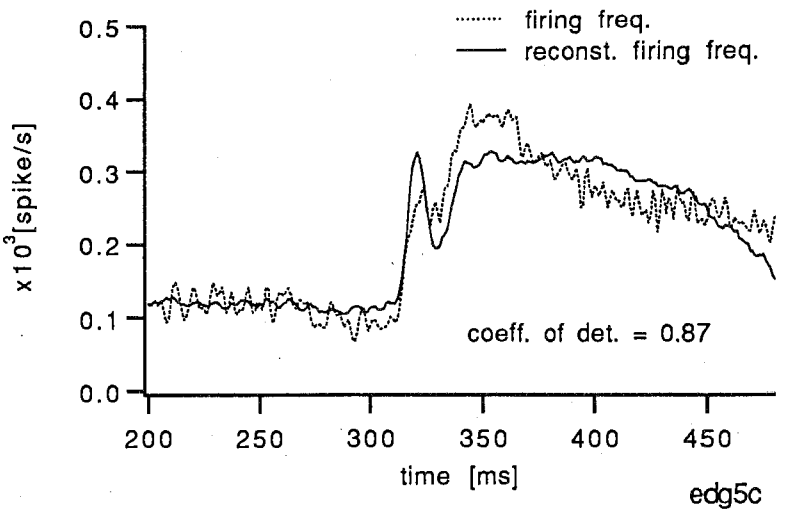
firing freq.
reconst. firing freq.
0.5
0.4
0.3
0.2
0.1
0.0
x10^3[spike/s]
coeff. of det. = 0.87
200
250
300
350
400
450
time [ms]
edg5c

Figure 10

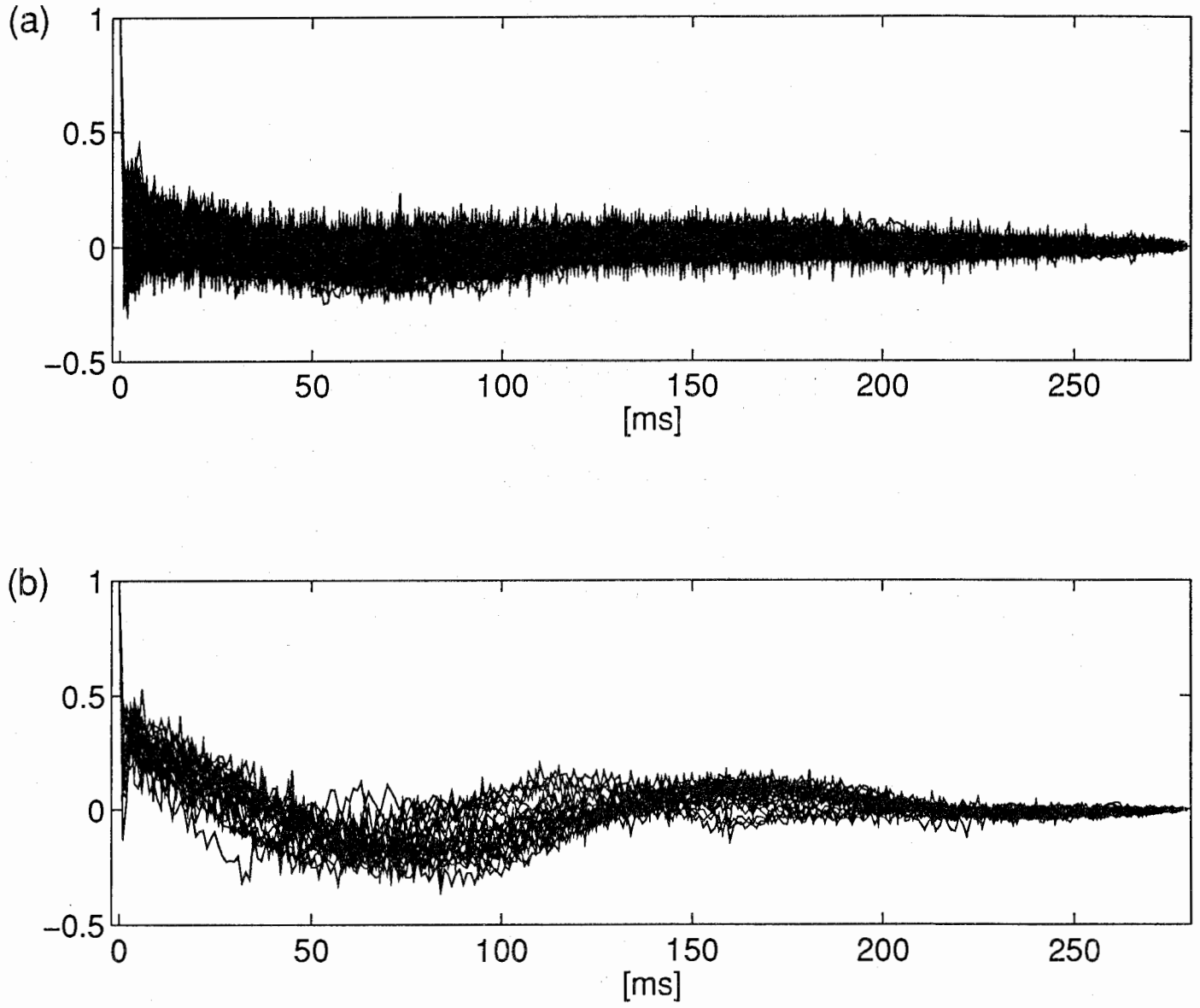

Figure 11

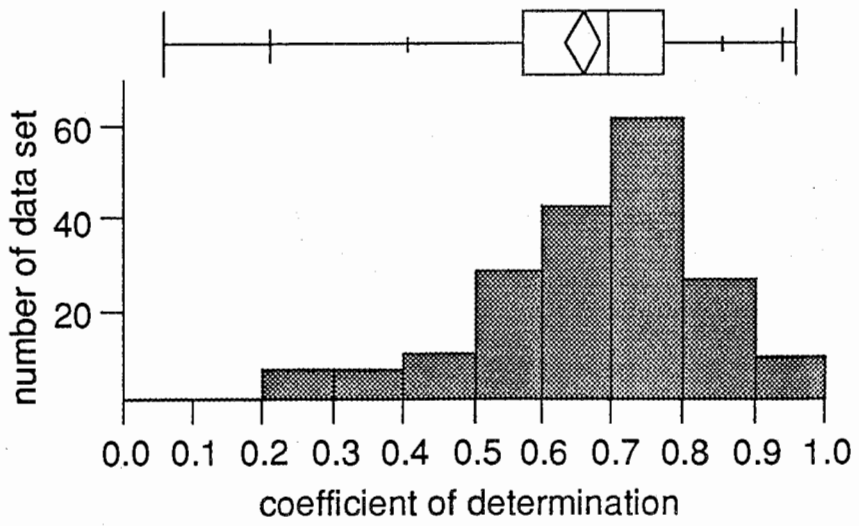
number of data set
60
40
20
0.0 0.1 0.2 0.3 0.4 0.5 0.6 0.7 0.8 0.9 1.0
coefficient of determination

Figure 12

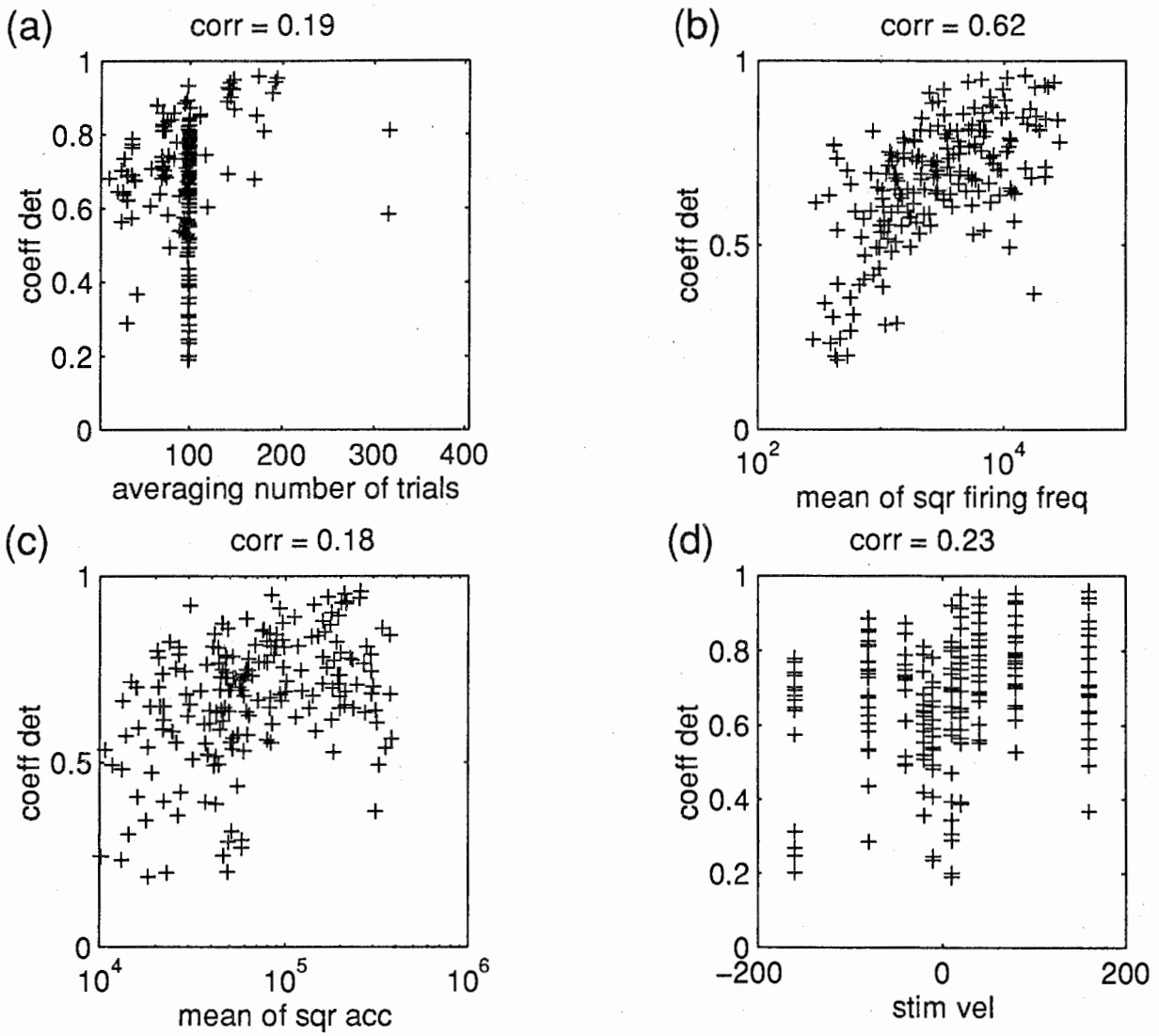
(a)
corr = 0.19
coeff det
averaging number of trials
(b)
corr = 0.62
coeff det
mean of sqr firing freq
(c)
corr = 0.18
coeff det
mean of sqr acc
(d)
corr = 0.23
coeff det
stim vel

Figure 13

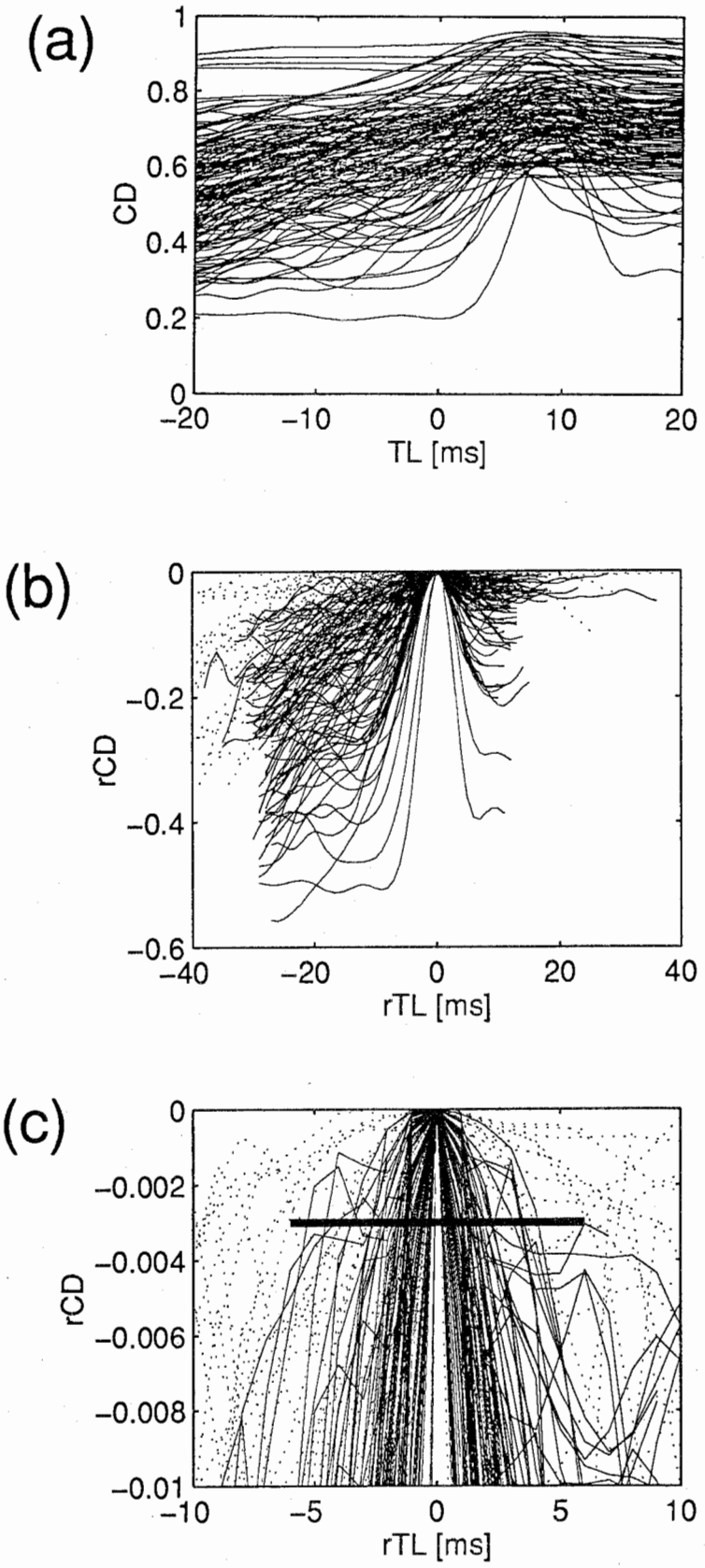

Figure 14

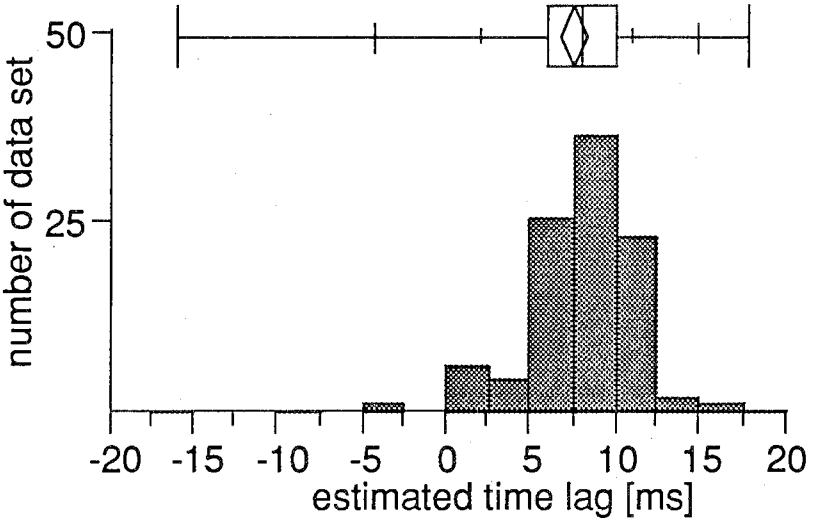

Figure 15

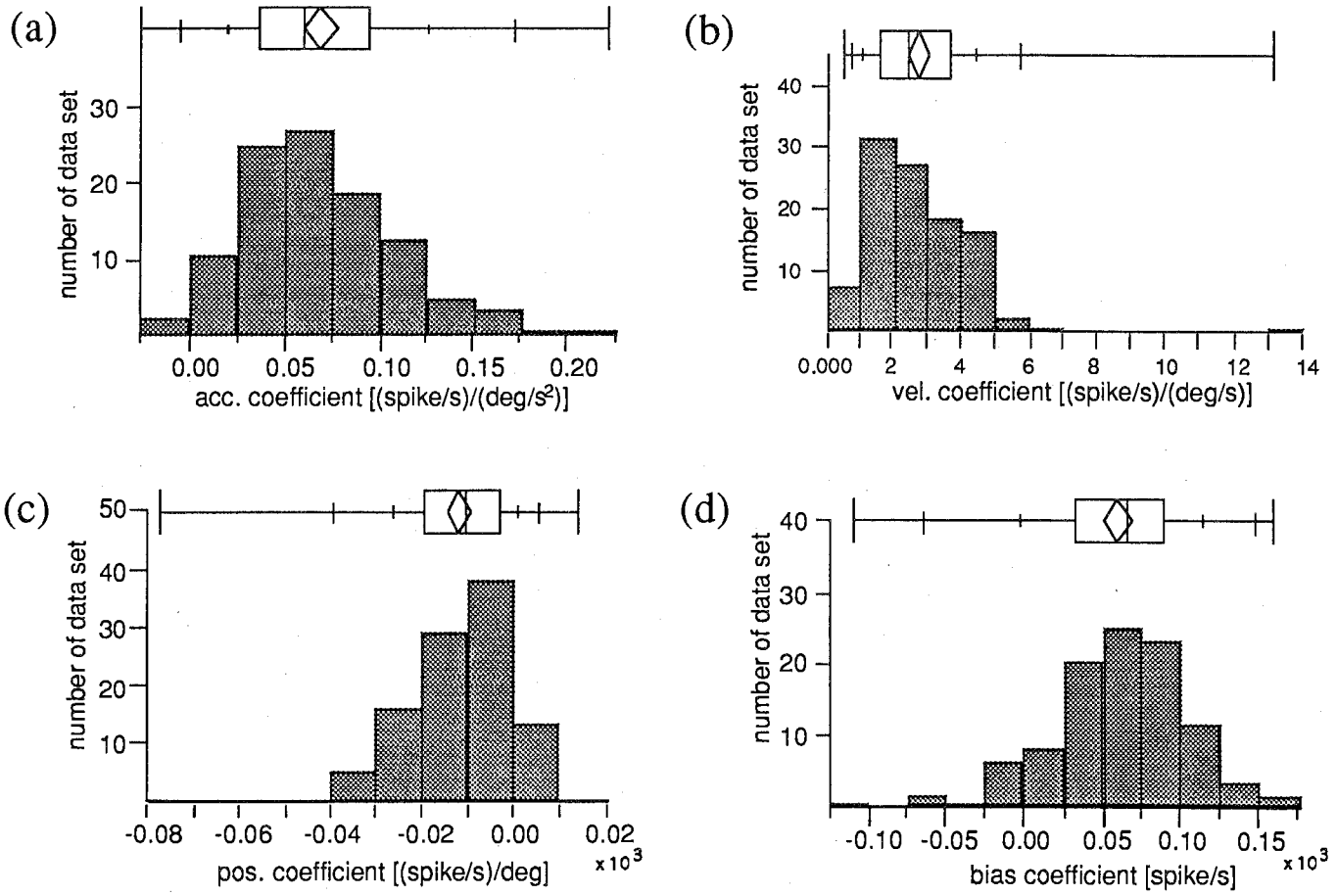

Figure 16

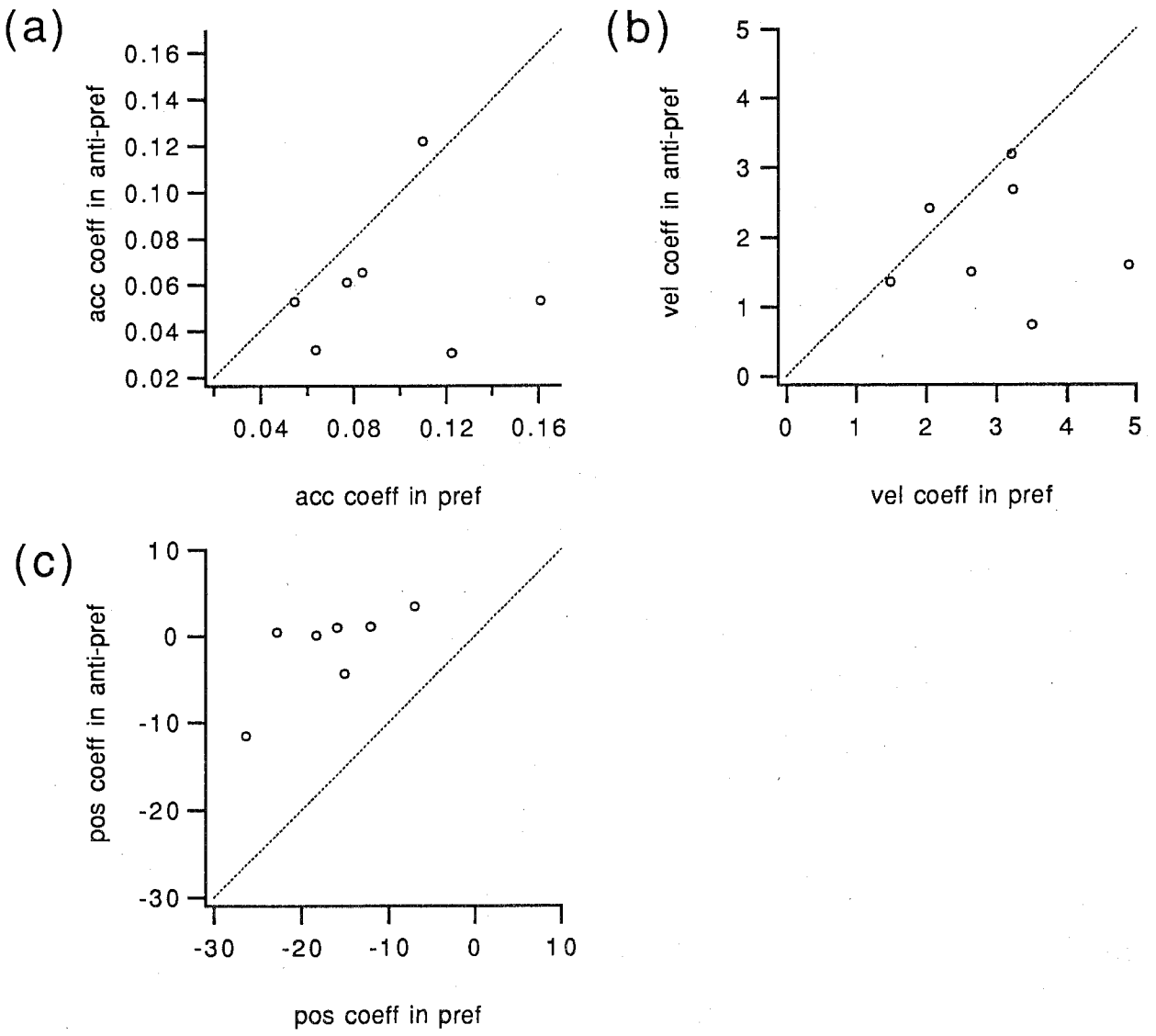
(a)
0.16
0.14
0.12
0.10
0.08
0.06
0.04
0.02
acc coeff in anti-pref
0.04
0.08
0.12
0.16
acc coeff in pref
(b)
5
4
3
2
1
0
vel coeff in anti-pref
0
1
2
3
4
5
vel coeff in pref
(c)
10
0
-10
-20
-30
pos coeff in anti-pref
-30
-20
-10
0
10
pos coeff in pref

Figure 17

(a)

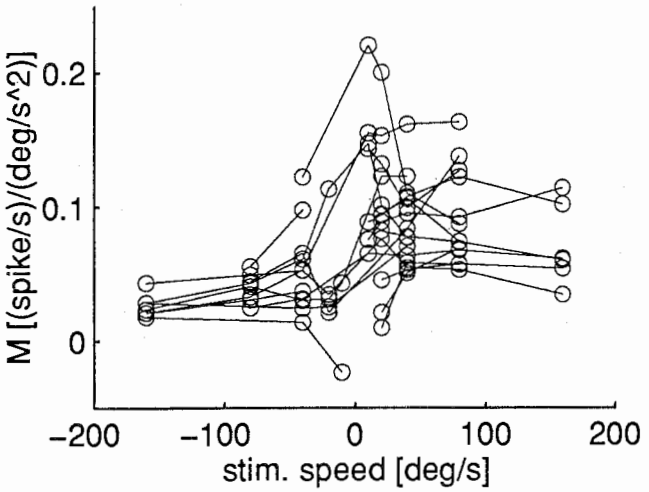

(b)

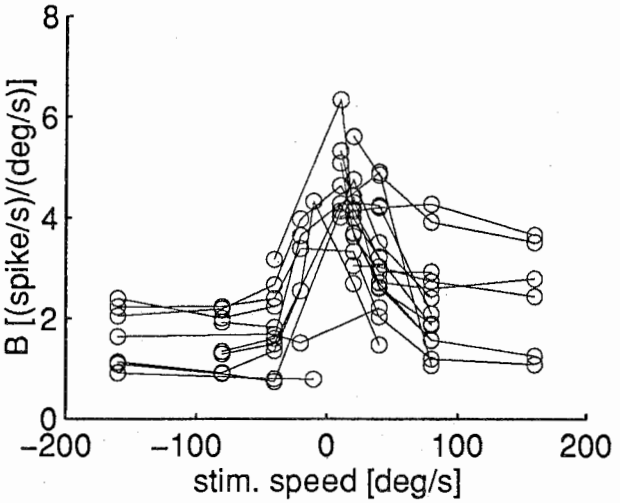

(c)

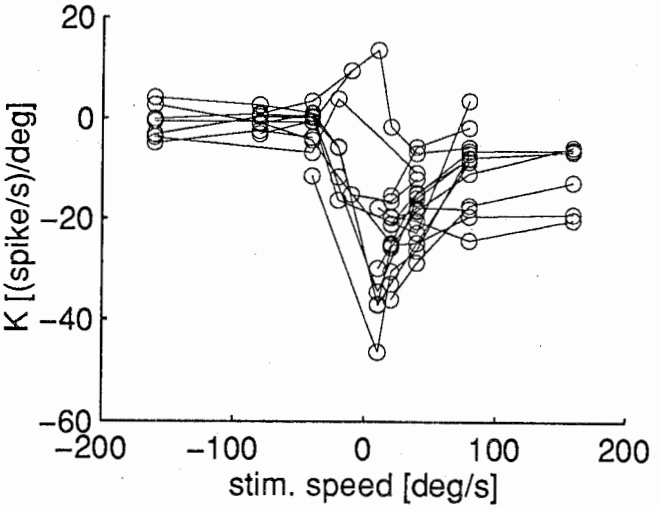

Figure 18

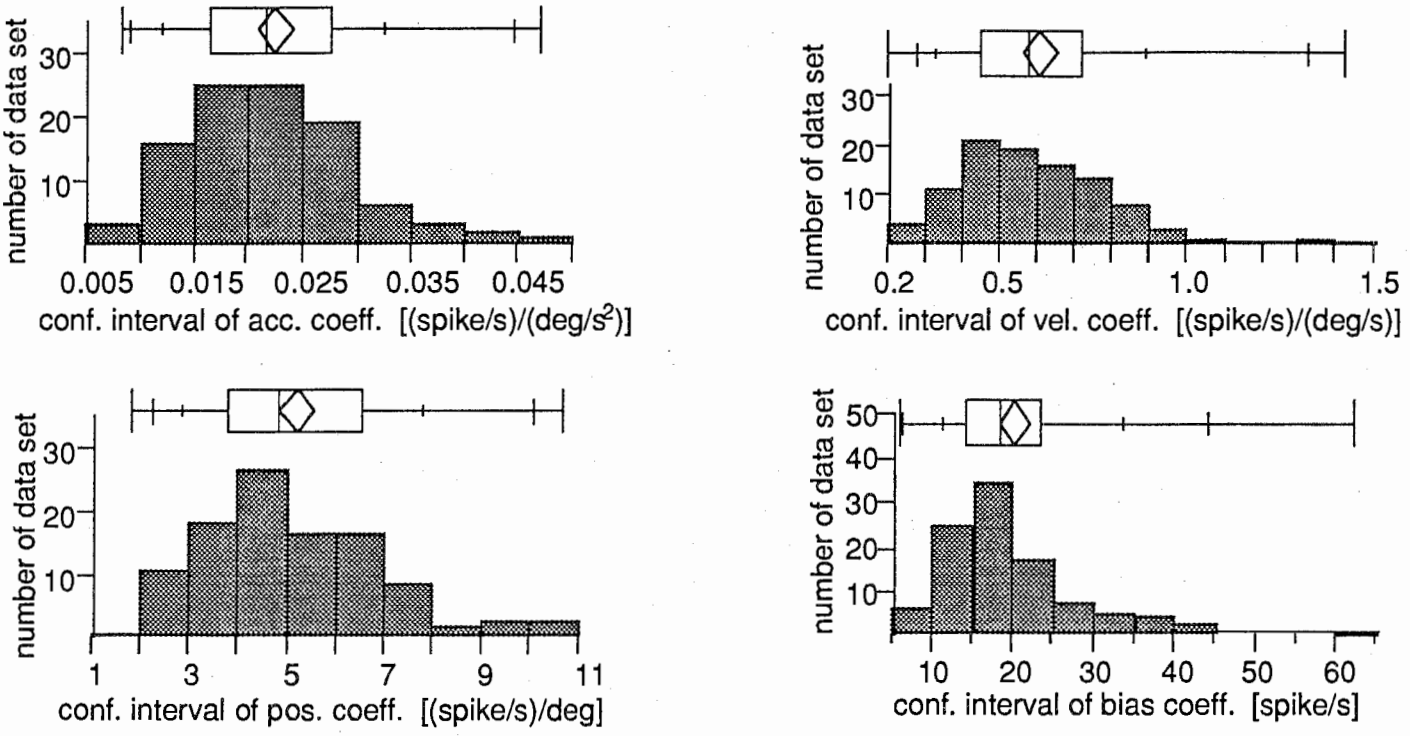
number of data set
30
20
10
0.005
0.015
0.025
0.035
0.045
conf. interval of acc. coeff. [(spike/s)/(deg/s²)]
number of data set
30
20
10
0.2
0.5
1.0
1.5
conf. interval of vel. coeff. [(spike/s)/(deg/s)]
number of data set
30
20
10
1
3
5
7
9
11
conf. interval of pos. coeff. [(spike/s)/deg]
number of data set
50
40
30
20
10
10
20
30
40
50
60
conf. interval of bias coeff. [spike/s]

Figure 19

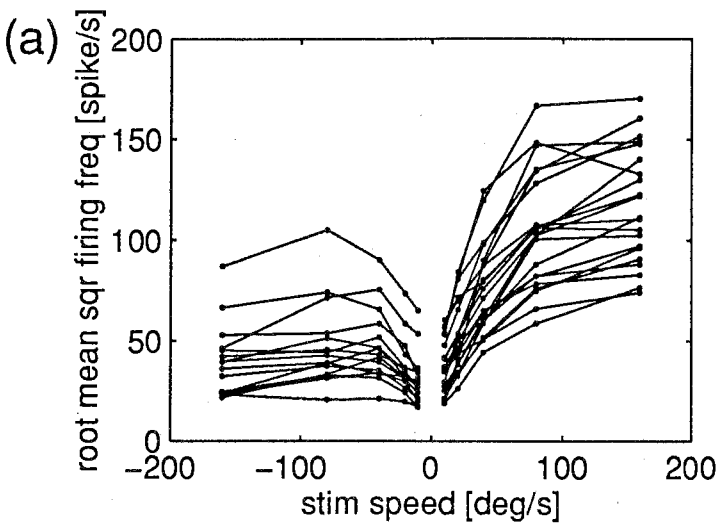
(a)
root mean sqr firing freq [spike/s]
200
150
100
50
0
−200
−100
0
100
200
stim speed [deg/s]

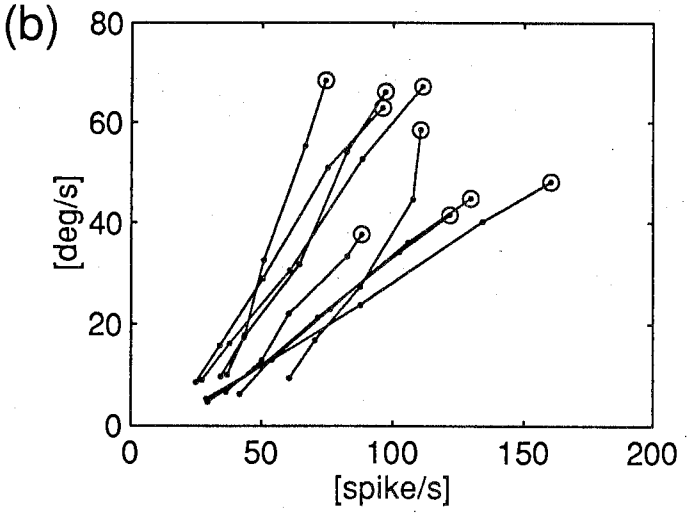
(b)
80
60
40
20
0
[deg/s]
0
50
100
150
200
[spike/s]

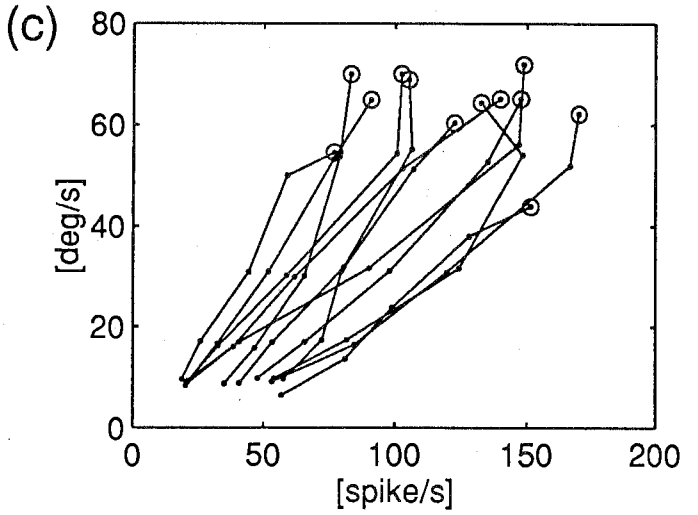
(c)
80
60
40
20
0
[deg/s]
0
50
100
150
200
[spike/s]

Figure 20

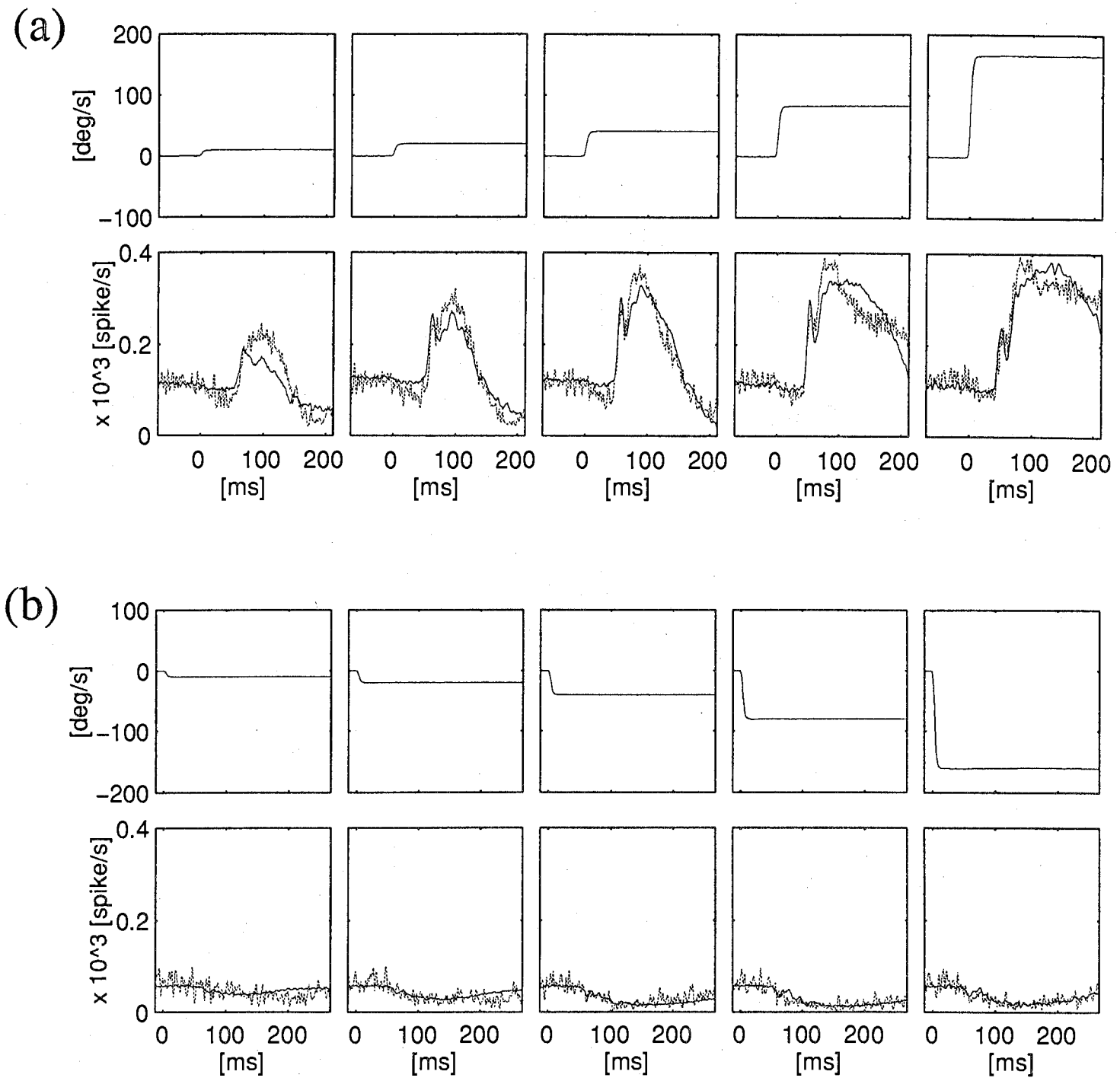
(a)
200
100
0
−100
[deg/s]
0.4
0.2
0
x 10^3 [spike/s]
0 100 200
[ms]
(b)
100
0
−100
−200
[deg/s]
0.4
0.2
0
x 10^3 [spike/s]
0 100 200
[ms]

Figure 21

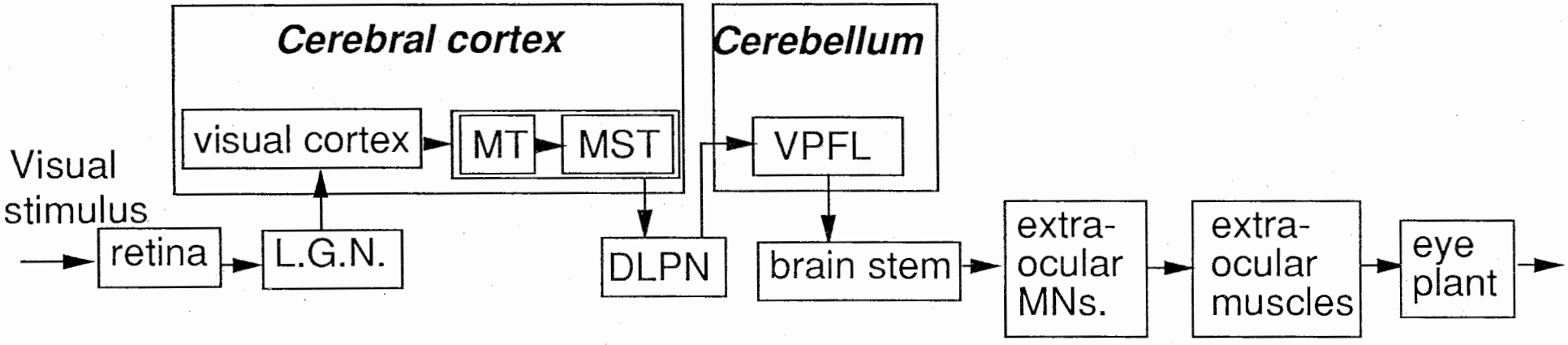
Cerebral cortex
Cerebellum
visual cortex
MT
MST
VPFL
Visual stimulus
retina
L.G.N.
DLPN
brain stem
extra-ocular MNs.
extra-ocular muscles
eye plant

Figure 22

Table 1

unit name	pref. speed (5 speeds) [deg/s]	anti-pref. speed (5 speeds) [deg/s]	duration (6 lengths) [ms]
ed16a	@		@
edg0b	@		
edg1e	80		
edg2b	@		
edg3f	10,20,40,80		
edg4a	@		
edg5c	@		
edg7b	@		
gc10a			@
gc15d			10, 20
kc38a	80		
kc38b	80	-80	
kc38c	80	-80	
kc40b	80	-80	
kc42a	@	@	
kc45a	80	-80	
kcg1c	@	@	
kcg2c	@	@	
kcg3d	@	@	
kcg4a	@	@	
kcg4b	@	@	
kcg4c	@	@	
kcg6g	@	@	
kcg7a	@	@	
kcg7b	@	@	@
kcg8c	@	@	
kcg9d	@	@	
kcgab	@	@	@
kcgbc	@	@	@
kcgcc	@	@	@
the number of cells	28	19	7
the number of patterns	115	79	38

Table 2

		number of data set (%)							
		prepared	accepted by bino. test	accepted by auto-corr test	accepted by CD test	accepted by time-lag test	accepted by strict sel.	accepted by loose sel.
speed condition deg/s	-160	15	10 (67)	14 (93)	10 (67)	13 (87)	4 (27)	7 (47)
	-80	19	10 (53)	18 (95)	15 (79)	14 (74)	5 (26)	10 (52)
	-40	15	10 (67)	15 (100)	12 (80)	15 (100)	7 (47)	12 (80)
	-20	15	11 (73)	14 (93)	9 (60)	10 (67)	3 (20)	5 (33)
	-10	15	13 (87)	15 (100)	6 (40)	8 (53)	1 (7)	2 (13)
	10	22	16 (73)	22 (100)	12 (55)	16 (73)	7 (32)	8 (36)
	20	22	20 (91)	22 (100)	16 (73)	19 (86)	11 (50)	13 (59)
	40	22	19 (86)	21 (95)	20 (91)	19 (86)	15 (68)	17 (77)
	80	28	23 (82)	23 (82)	26 (93)	21 (75)	15 (54)	15 (54)
	160	21	14 (67)	10 (48)	17 (81)	13 (62)	6 (29)	6 (29)
duration condition ms	10	7	5 (71)	7 (100)	2 (29)	7 (100)	2 (29)	2 (29)
	20	7	4 (57)	7 (100)	4 (57)	6 (86)	4 (57)	4 (57)
	40	6	6 (100)	5 (83)	3 (50)	3 (50)	3 (50)	2 (33)
	60	6	4 (67)	5 (83)	4 (67)	4 (67)	2 (33)	2 (33)
	80	6	5 (83)	5 (83)	5 (83)	3 (50)	2 (33)	2 (33)
	160	6	5 (83)	5 (83)	6 (100)	3 (50)	2 (33)	2 (33)
	total	232	175/232	208/232	167/232	174/232	89/232	109/232

Table 3.1

	averaged estimated coefficients and time-lag	
	ave. of 109 data sets (loose test condition)	ave. of 89 data sets (strict test condition)
M [(spike/s)/(deg/s^2)]	0.0694 (±0.0434 S.D.)	0.0751 (±0.0416 S.D.)
B [(spike/s)/ (deg/s)]	2.76 (±1.63 S.D.)	2.86 (±1.79 S.D.)
K [(spike/s)/deg]	-12.2 (±12.8 S.D.)	-13.7 (±13.1 S.D.)
f bias [spike/s]	60.2 (±46.1 S.D.)	65.5 (±51.6 S.D.)
δ [ms]	7.50 (±4.24 S.D.)	7.79 (±3.64 S.D.)

Table 3.2

	averaged estimated coefficients and time-lag of 109 data sets		
	preferred direction (59)	anti-preferred direction (36)	stimulus duration change (14)
M [(spike/s)/(deg/s^2)]	0.0882 (±0.0446 S.D.)	0.0409 (±0.0270 S.D.)	0.0633 (±0.0304 S.D.)
B [(spike/s)/ (deg/s)]	3.39 (±1.79 S.D.)	1.94 (±0.91 S.D.)	2.24 (±1.31 S.D.)
K [(spike/s)/deg]	-18.0 (±13.5 S.D.)	-2.32 (±5.32 S.D.)	-13.3 (±6.32 S.D.)
f bias [spike/s]	56.1 (±47.6 S.D.)	74.7 (±37.4 S.D.)	40.0 (±51.5 S.D.)
δ [ms]	8.51 (±1.99 S.D.)	5.53 (±6.45 S.D.)	8.29 (±1.90 S.D.)

Table 4

	Number of data set in each range of *p*value of t-test		
	$p < 0.005$	$0.005 < p < 0.05$	$0.05 < p$
jerk component	12	12	89
acc. component	101	3	9
vel. component	112	1	0
pos. component	95	3	15
bias component	100	3	10

Table 5

stim. condition	number of data set						
	prepared	accepted by bino. test	accepted by auto-corr test	accepted by CD test	accepted by lag test	accepted by strict sel.	accepted by loose sel.
pref dir	21	3	13	18	16	2	9
anti-pref dir	15	6	11	5	8	2	3
duration	6	1	5	6	3	1	2
pref + anit-pref	15	0	5	14	8	0	1
pref + duration	5	0	2	4	2	0	1

Table 6

	averaged estimated coefficients and time-lag chosen by loose sel.		
	pref.	anti-pref.	duration
M [(spike/s)/(deg/s^2)]	0.0666	0.0320	0.0740
B [(spike/s)/ (deg/s)]	2.63	2.21	2.79
K [(spike/s)/deg]	-15.1	-4.12	-6.09
f bias [spike/s]	71.2	74.7	78.1
δ [ms]	7.33	6.00	9.00